Short Article

Cell Metabolism

Tanycytes Regulate Lipid Homeostasis by Sensing Free Fatty Acids and Signaling to Key Hypothalamic Neuronal Populations via FGF21 Secretion

Graphical Abstract

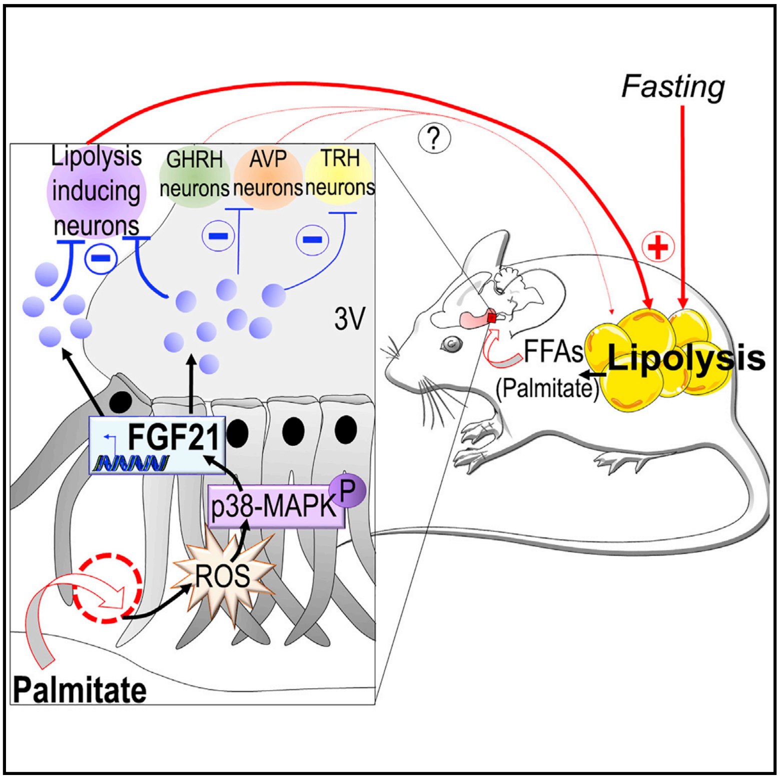

Authors

Sarah Geller, Yoan Arribat, Citlalli Netzahualcoyotzi, ..., Francesca Amati, Isabel C. Lopez-Mejia, Luc Pellerin

Correspondence

sarah.geller.phd@gmail.com (S.G.), luc.pellerin@unil.ch (L.P.)

In Brief

In obesity, the increased levels of circulating lipids induce metabolic dysfunction. Thus, it is essential to determine the mechanisms behind fat storage. Here, Geller et al. demonstrate that brain-specific glial cells, the tanycytes, sense circulating lipid levels to regulate body fat storage via the production of Fgf21.

Highlights

- Hypothalamic tanycytes synthesize and secrete Fgf21 under nutritional stress
- Palmitate oxidation in tanycytes triggers Fgf21 expression via the ROS/p38-MAPK pathway
- Deletion of tanycytic Fgf21 reduces fat depot size and promotes energy expenditure
- Deletion of tanycytic Fgf21 promotes lipolysis and browning of WAT

Geller et al., 2019, Cell Metabolism *30*, 833–844
October 1, 2019
https://doi.org/10.1016/j.cmet.2019.08.004

Cell Metabolism
Short Article

Tanycytes Regulate Lipid Homeostasis by Sensing Free Fatty Acids and Signaling to Key Hypothalamic Neuronal Populations via FGF21 Secretion

Sarah Geller,[1,*] Yoan Arribat,[1] Citlalli Netzahualcoyotzi,[1] Sylviane Lagarrigue,[1] Lionel Carneiro,[1] Lianjun Zhang,[2,7] Francesca Amati,[1,3,4] Isabel C. Lopez-Mejia,[5] and Luc Pellerin[1,6,8,*]
[1]Department of Physiology, University of Lausanne, 1005 Lausanne, Switzerland
[2]Ludwig Center for Cancer Research, University of Lausanne, 1066 Epalinges, Switzerland
[3]Institute of Sports Sciences, University of Lausanne, Lausanne 1005, Switzerland
[4]Service of Endocrinology, Diabetology, and Metabolism, Department of Medicine, Lausanne University Hospital, Lausanne 1011, Switzerland
[5]Center for Integrative Genomics, University of Lausanne, 1015 Lausanne, Switzerland
[6]Centre de Résonance Magnétique des Systèmes Biologiques, UMR5536 CNRS, LabEx TRAIL-IBIO, Université de Bordeaux, Bordeaux Cedex 33760, France
[7]Present address: Suzhou Institute of Systems Medicine, Chinese Academy of Medical Sciences and Peking Union Medical College, Center for Systems Medicine, Suzhou, China
[8]Lead Contact
*Correspondence: sarah.geller.phd@gmail.com (S.G.), luc.pellerin@unil.ch (L.P.)
https://doi.org/10.1016/j.cmet.2019.08.004

SUMMARY

The hypothalamus plays a key role in the detection of energy substrates to regulate energy homeostasis. Tanycytes, the hypothalamic ependymo-glia, are located at a privileged position to integrate multiple peripheral inputs. We observed that tanycytes produce and secrete Fgf21 and are located close to Fgf21-sensitive neurons. Fasting, likely via the increase in circulating fatty acids, regulates this central *Fgf21* production. Tanycytes store palmitate in lipid droplets and oxidize it, leading to the activation of a reactive oxygen species (ROS)/p38-MAPK signaling pathway, which is essential for tanycytic Fgf21 expression upon palmitate exposure. Tanycytic Fgf21 deletion triggers an increase in lipolysis, likely due to impaired inhibition of key neurons during fasting. Mice deleted for tanycytic Fgf21 exhibit increased energy expenditure and a reduction in fat mass gain, reminiscent of a browning phenotype. Our results suggest that tanycytes sense free fatty acids to maintain body lipid homeostasis through Fgf21 signaling within the hypothalamus.

INTRODUCTION

Fibroblast growth factor 21 (Fgf21) is a metabolic hormone expressed by many tissues (muscle and white and brown adipose tissues [WAT and BAT, respectively]) but abundantly by the liver (Staiger et al., 2017). Nutrient deprivation, fasting, lipid intake, or a ketogenic diet induce an increase in circulating Fgf21. Fgf21 was proposed as an energy stress signal improving lipid and glucose metabolism via a direct action on peripheral tissues and in the central nervous system (CNS) (Guan et al., 2016; Sa-Nguanmoo et al., 2016). Both pre-clinical and clinical studies revealed increased serum Fgf21 levels in rodents and patients with metabolic diseases (e.g., obesity) (Zhang et al., 2015). This metabolic signal represents a potential treatment for diabetes and other metabolic diseases (Guan et al., 2016).

Fgf21 is detected in the cerebrospinal fluid (CSF), and the brain expresses Fgf21 receptors (FGFRs), as well as their co-receptor β-Klotho (Sa-Nguanmoo et al., 2016). In the hypothalamus, Fgf21 signaling regulates hepatic glucose production and other peripheral functions under physiological conditions (Bookout et al., 2013; Owen et al., 2013; Talukdar et al., 2016; von Holstein-Rathlou et al., 2016). Peripheral Fgf21 acts in the hypothalamus after crossing the blood-brain barrier by simple diffusion or extravasates from the fenestrated capillaries into the hypothalamus (Hsuchou et al., 2007; Xu et al., 2017). In addition, Fgf21 might be produced by the hypothalamus as a function

Context and Significance

The brain plays an important role in maintaining energy balance. Researchers at the University of Lausanne in Switzerland found that a specific type of brain cells, called tanycytes, sense energy deprivation during fasting and release the metabolic hormone FGF21 to trigger energy-sparing countermeasures such as fat accumulation and glucose production in fat tissues and the liver, respectively. These results highlight the complex interplay between the brain and other organs and can inform our decisions in the treatment of metabolic diseases.

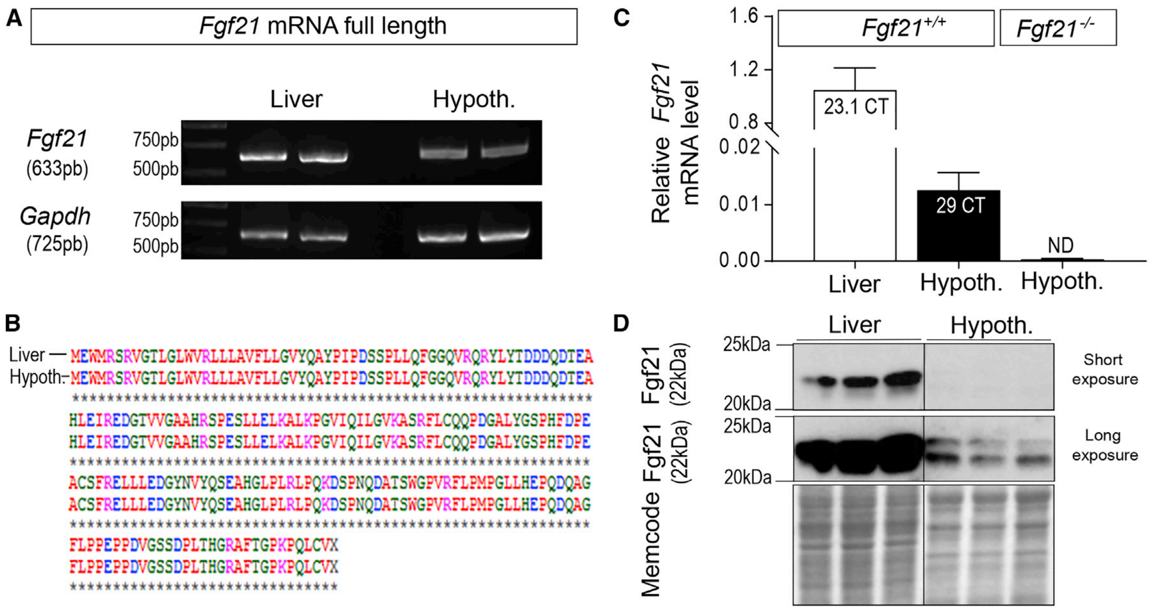

Figure 1. Identification of the Fgf21 Isoform Produced in the Hypothalamus

(A) RT-PCR analysis of full-length transcripts expressed in hypothalamus and liver.

(B) Comparative alignment of Fgf21 protein sequences from liver and hypothalamus.

(C) RT-qPCR analysis of *Fgf21* expression levels in liver and hypothalamus of WT and $Fgf21^{-/-}$ mice (relative to Poly2a 27.4 CT, n = 6/group).

(D) Representative western blots of Fgf21 in hypothalamus and liver after two exposure times. Values indicate means ± SEM. See also Figure S1.

of the metabolic status. As a major metabolic sensing area, the hypothalamus dialogues with peripheral tissues and regulates energy homeostasis, in particular peripheral glucose and lipid metabolism (Carneiro et al., 2016; Leloup et al., 2016; Waterson and Horvath, 2015).

We show here that (1) tanycytes, a subset of hypothalamic glial cells, produce and secrete Fgf21; (2) fasting-induced energy substrate release, such as palmitate (Jensen et al., 1987), regulates the central production of Fgf21 by tanycytes via a reactive oxygen species (ROS)/p38-MAPK signaling pathway; and (3) tanycytic Fgf21 participates in the central regulation of lipid homeostasis, likely via an action on GHRH, TRH, and AVP neurons.

RESULTS AND DISCUSSION

Fgf21 Is Synthesized within the Hypothalamus

RT-PCR and sequence analysis revealed the presence of an Fgf21 full-length transcript in the hypothalamus of mice fed *ad libitum* (Figures 1A and 1B). Sequence analysis demonstrated that the hypothalamus expresses the same isoform as the liver. qPCR analysis confirmed the hypothalamic expression of Fgf21 mRNA in $Fgf21^{+/+}$ mice, albeit at lower levels than in the liver. No *Fgf21* mRNA was detected in the hypothalamus from $Fgf21^{-/-}$ mice (Figure 1C). Western blot analysis confirmed a moderate hypothalamic expression of the peptide but lower than in the liver (Figures 1D and S1).

A central production of Fgf21 has been suggested (Sa-Nguanmoo et al., 2016; Staiger et al., 2017; Zhang et al., 2012). Fgf21 was detected by western blot in several brain areas (Mäkelä et al., 2014). However, it could be an accumulation of hepatic Fgf21 (Liang et al., 2014). *Fgf21* expression was detected in mouse and human brain (Petryszak et al., 2016) and in the cortex and hippocampus of mice following mitochondrial dysfunction (Restelli et al., 2018). Our data prove hypothalamic Fgf21 production and raise the question of its site(s) of action (autocrine or paracrine). Some evidence points toward a local action for hypothalamic Fgf21: (1) the Fgf21 co-receptor β-Klotho (*Klb*) (Figure S1E); (2) the *Fgfr1c* receptor (Figure S1F), both are expressed in the hypothalamus (Talukdar et al., 2016); and (3) c-fos is induced in the hypothalamus after Fgf21 injection (Yang et al., 2012).

Hypothalamic Tanycytes Produce and Secrete Fgf21 According to Nutritional Status

To identify the hypothalamic area(s) producing Fgf21, punches were made of different regions known to be sensitive to *Fgf21* (Fon Tacer et al., 2010; Liang et al., 2014; Xu et al., 2017). We detected *Klb* mRNA and *Fgfr1c* mRNA in all these hypothalamic areas (Figures S1H and S1I). *Fgf21* mRNA is highly expressed in the median eminence/medial basal hypothalamus (ME/MBH), in particular along the lower part of the third ventricle (3V) (Figures 2A, 2B, and S2). Immunofluorescence performed on fed mice showed strong Fgf21 immunoreactivity (IR) in the ME (Figures 2C, S1, and S3). A weak labeling was observed along the arcuate nucleus (ARC) (arrows, Figures 2C and S1). Fgf21-IR was detected in close proximity to neuronal (Figures S2E–S2G) and astrocytic markers (Figure S2H), but co-labeling was only detected with the tanycytic marker vimentin, as seen in cell bodies of tanycytes, along the 3V (arrowheads), and in tanycyte end-feet that extend in the ME (arrows, Figure 2D).

An *in vitro* mouse model of tanycytes was developed to study their Fgf21 production. Immuno-detection of tanycytic markers

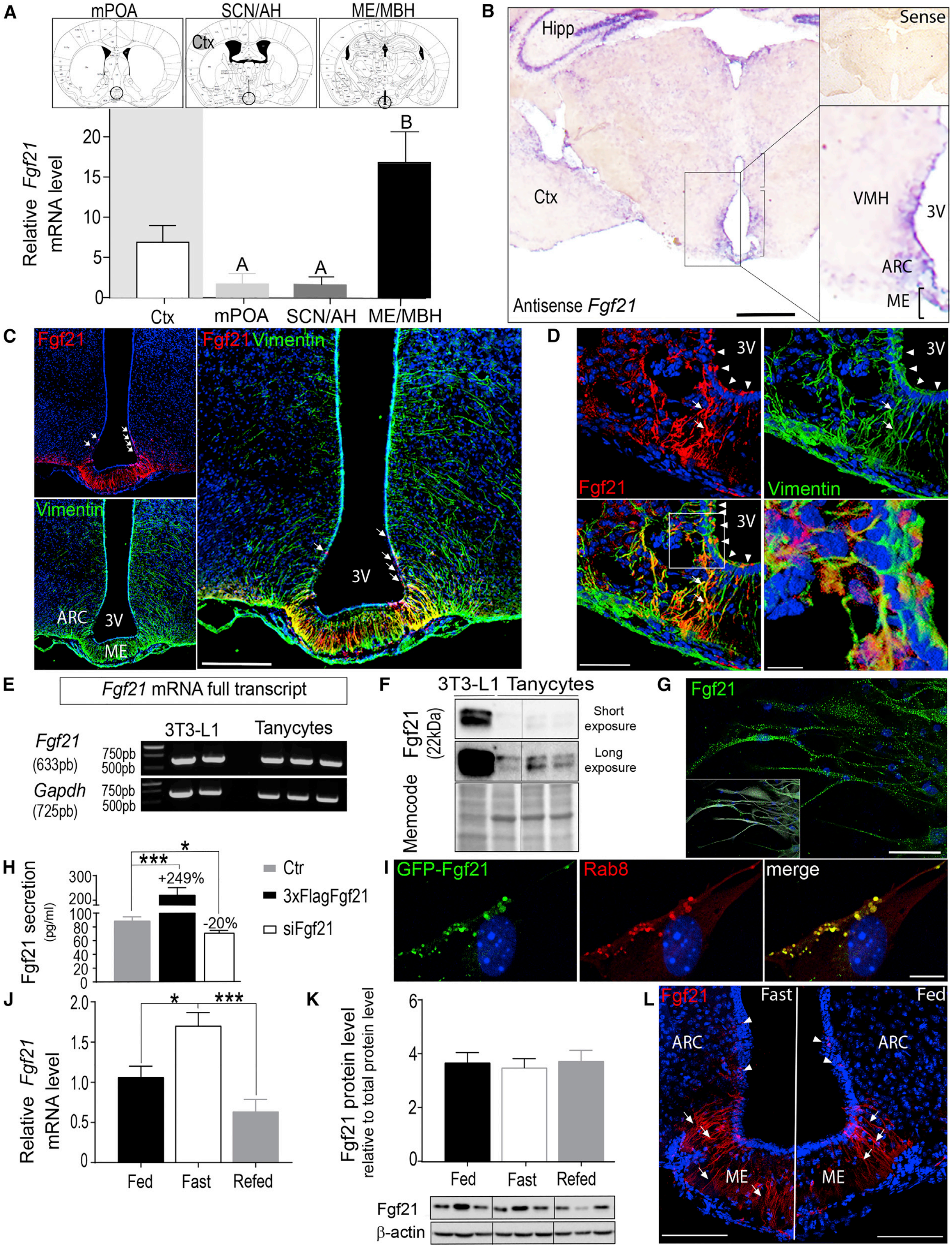

Figure 2. Characterization of the Expression and Secretion of Fgf21 by Hypothalamic Tanycytes *In Vivo* and *In Vitro*

(A) *Fgf21* mRNA levels in cortex and different hypothalamic areas identified on schematic brain sections in the top panel (relative fold change to SCN/AH, n = 6/group).

(legend continued on next page)

and the absence of neuronal (NeuN) and astrocytic (GS) marker expression confirmed culture enrichment (Figures S3A–S3C). Cultured tanycytes expressed the full-length *Fgf21* transcript and produced the Fgf21 peptide, like 3T3-L1 adipocytes (Figures 2E and 2F). Fgf21 immunolabeling confirmed the presence of Fgf21 peptide in tanycyte end-feet and cell bodies, around the nucleus (Figure 2G), as observed *in vivo*. Our *in vivo* results in ARC/VMH tanycytes and the punctiform immunolabeling of Fgf21 *in vitro* raised the question of the presence of this peptide in secretory vesicles. Confocal analysis confirmed GFP-Fgf21 localization in tanycytes and showed co-localization of GFP-Fgf21 with Rab8, an exocytotic vesicle marker (Figure 2I). These data suggest that tanycytes secrete Fgf21, also confirmed by ELISA using culture supernatant (Figure 2H). Fgf21 silencing using small interfering RNA (siRNA) (Figures S3D and S3E) or Fgf21 overexpression (Figure S3F) induced a significant decrease and increase of Fgf21 secretion, respectively (Figure 2H), suggesting that the level of Fgf21 secretion is correlated with the level of Fgf21 expression in tanycytes. Tanycyte-secreted Fgf21 could act directly on neighboring Klb+ neurons or diffuse to more distant brain areas through the CSF, as described for leptin (Balland et al., 2014).

Fgf21 was reported to exert effects via the hypothalamus upon starvation, and a role for tanycytes in the adaptive response to fasting has been proposed (Langlet et al., 2013). Therefore, we compared hypothalamic Fgf21 expression between mice deprived of food for 24 h, mice refed for 6 h after a 24 h fast, and *ad libitum* fed mice (Figures 2 and S3). Fasting induced a significant increase of *Fgf21* mRNA expression, while refeeding significantly reduced it (Figure 2J). Hypothalamic Fgf21 protein levels did not vary with the nutritional status, while hepatic Fgf21 levels varied at both the mRNA and protein levels depending on nutritional status (Figures 2K, S3I, and S3J). These results are consistent with our *in vitro* data showing that tanycytic Fgf21 secretion increases proportionally to its production, resulting in no cellular accumulation. Indeed, fasting did not modify Fgf21-IR, either in ME (arrows) or in ARC (arrowheads, Figure 2K), suggesting that tanycytes do not accumulate (but most likely strongly secrete) Fgf21 upon fasting.

Palmitate Oxidation by Tanycytes Modulates *Fgf21* Expression and Secretion via ROS/p38-MAPK Signaling

The effect of fasting on hypothalamic *Fgf21* expression suggests that a circulating stimulus acts on the hypothalamus upon nutrient deprivation. Tanycytes occupy a privileged position to monitor blood-borne signals, such as hormones or metabolites (Langlet et al., 2013). In the fasting state, levels of free fatty acids (FFAs) increase in both blood and brain (Karmi et al., 2010; Le Foll and Levin, 2016). The effect of unsaturated (oleate) and saturated (palmitate) FAs on *Fgf21* mRNA expression was tested on primary cultures of tanycytes (Figures 3 and S4A). Palmitate, unlike oleate, caused a time-dependent increase in *Fgf21* mRNA expression (Figures 3A and S4A). Strikingly, the profile of *Fgf21* mRNA expression under palmitate stimulation correlated with Fgf21 secretion, peaking 12 h post-treatment (Figures 3A and 3B). Intravenous (i.v.) injections of palmitate induced a significant increase of *Fgf21* mRNA expression in ME/MBH punches isolated from mice 20 h post-injection (Figure 3C), supporting our *in vitro* results.

A recent report suggested that in muscle, FA β-oxidation (FAO) regulates *Fgf21* expression (Vandanmagsar et al., 2016). We determined in tanycytes the lipid droplet (LD) content in presence of palmitate alone or together with etomoxir, a mitochondrial FA uptake inhibitor (Figure 3D). LDs were detected in cell bodies and end-feet (arrows) of tanycytes 2 h after palmitate exposure. Etomoxir- and palmitate-treated cells contained even more LDs, mostly in cell bodies, suggesting an accumulation of lipids in the absence of FAO. Seahorse experiments revealed that tanycytes increased their oxygen consumption rate (OCR) after palmitate injection (Figures 3E and 3F), whereas etomoxir strongly reduced palmitate-dependent respiration. Since *Fgf21* expression was shown to depend on ROS production and p38-MAPK signaling in muscle and adipocytes (Jeanson et al., 2016; Ribas et al., 2014), we studied the capacity of tanycytes to produce ROS, activate p38-MAPK, and express *Fgf21* in response to palmitate (Figures 3G–3N). Time-lapse analysis showed that palmitate induces an increase of ROS-dependent dichlorofluorescein (DCF) fluorescence in tanycytes (arrows, Figure 3G). This significant elevation of ROS production by tanycytes was maintained 3 h after palmitate addition and was prevented by the antioxidant N-acetyl-L-cysteine (NAC) (Figure 3H). The presence of NAC blunted *Fgf21* mRNA induction in response to palmitate (Figure 3I). These observations suggest that during fasting, palmitate oxidation by tanycytes induces *Fgf21* mRNA expression through ROS production. ROS have been shown to play a signaling role in the regulation of food intake by the hypothalamus (Drougard et al., 2015) and in glucose sensing by hypothalamic astrocytes (Leloup et al., 2016). We identified a new role for ROS signaling in a lipid-sensing pathway involving tanycytes.

In order to understand the mechanism, the influence of palmitate on p38-MAPK phosphorylation was investigated

(B) *Fgf21* mRNA distribution in frontal brain sections. The bottom right panel shows higher magnification. Top right panel illustrates the negative control.
(C and D) Low magnification (C) and high magnification (D) of Fgf21-IR and Vimentin-IR (tanycyte marker) along the 3V (C) and in median eminence (D).
(E and F) RT-PCR analysis of *Fgf21* full-length transcript (E) and representative western blots for Fgf21 peptide (F) in primary cultures of mouse tanycytes and in 3T3-L1 adipocytes.
(G) Fgf21-IR in cultured tanycytes.
(H) Mean concentration of Fgf21 secreted by tanycytes cultured in control conditions, after Fgf21 overexpression (3xFlag-Fgf21) or after Fgf21 silencing (si*Fgf21*).
(I) Focal plane showing GFP-Fgf21 in Rab8 immunoreactive vesicles, in cultured tanycytes.
(J and K) Graphs representing mRNA (J) and protein (K) expression levels of hypothalamic Fgf21 from WT mice in fed, fasted (24 h), and refed (6 h) states (n = 8/group).
(L) Representative photomicrographs showing FGF21-IR in the ME of mice in fed and fasted states. Scale bars, 1 mm (B), 200 μm (C), 50 μm (D and G), 15 μm (I), and 100 μm (L). One-way ANOVA was performed followed by Tukey's HSD test for multiple comparisons (A versus B), $p < 0.05$ (A), or followed by Dunnett's test for multiple comparisons with the control (H) or with fasted state (J and K), *$p < 0.05$; ***$p < 0.001$. Values indicate means ± SEM. See also Figures S1–S3.

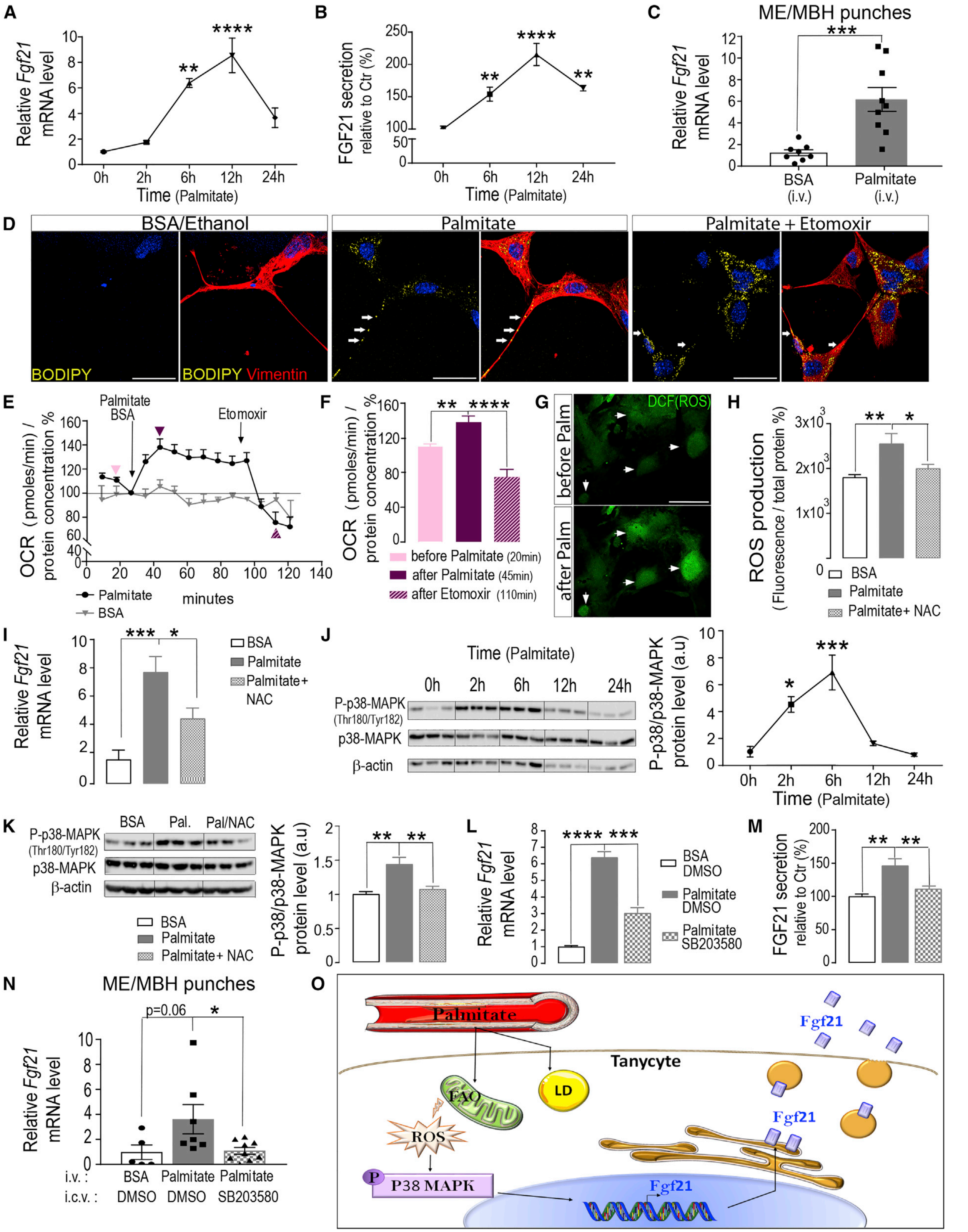

(legend on next page)

in vitro. Palmitate, but not oleate, enhanced p38-MAPK phosphorylation 2 and 6 h post-treatment (Figure 3J), preceding palmitate-induced *Fgf21* expression (Figures 3A and S4B). NAC prevented the effect of palmitate on p38-MAPK phosphorylation (Figure 3K), suggesting that ROS production is necessary for the activation of p38-MAPK and therefore for Fgf21 production. It is noteworthy that saturated FAs, like palmitate, have been shown to be more powerful inducers of ROS production than unsaturated FAs, like oleate (Ly et al., 2017). Consistent with our hypothesis, the use of SB203580, a p38-MAPK inhibitor, prevented palmitate-induced *Fgf21* expression and secretion in cultured tanycytes (Figures 3L and 3M). Intracerebroventricular SB203580 injection in the 3V, 1 h before palmitate i.v. injection, prevented the effect of palmitate on *Fgf21* mRNA expression in ME/MBH punches (Figure 3N), demonstrating that palmitate-induced Fgf21 production in tanycytes requires the activation of the ROS/p38-MAPK pathway (Figure 3O).

In fasting conditions, β-hydroxybutyrate (BHB) and lactate levels increase (Pan et al., 2000; Violante et al., 2009) and can be sensed by the hypothalamus (Carneiro et al., 2016; Kokorovic et al., 2009). In addition, BHB and lactate promote *Fgf21* expression in adipocytes (Jeanson et al., 2016). We found that lactate, but not BHB, increased *Fgf21* mRNA expression in cultured tanycytes (Figures S4C–S4E). Although lactate-induced *Fgf21* expression involves p38-MAPK signaling in adipocytes (Jeanson et al., 2016), we did not observe such an effect in cultured tanycytes (Figure S4F). These results emphasize that tanycytes sense nutrients and modulate Fgf21 production, although the signaling mechanisms seem nutrient-specific. Oh et al. (2012) observed that specific FFAs modulate distinct cellular functions and proposed a "division of labor" between different FFA-sensing mechanisms: regulation of energy balance (by oleate) versus regulation of fuel storage or mobilization via the hypothalamic-pituitary-adrenal (HPA) axis (by palmitate). Our data suggest that palmitate-dependent tanycytic Fgf21 production could be the link between hypothalamic lipid sensing and peripheral lipid mobilization.

Tanycytic Fgf21 Deletion Alters Peripheral Lipid and Glucose Metabolism, Likely by Relieving Inhibition of Lipolysis-Inducing Hypothalamic Neurons

To explore the role of hypothalamic Fgf21 in whole-body energy homeostasis, we deleted Fgf21 in tanycytes using a Cre-lox strategy. Injection of TAT-CRE recombinase in the 3V allowed us to preferentially target tanycytes (Langlet et al., 2013) as verified using tdTomato$^{fl/fl}$ mice (Figure 4A). In *Fgf21*$^{fl/fl}$ mice, TAT-CRE injection caused a strong decrease of hypothalamic Fgf21 mRNA expression (Figure 4B). Deletion of hypothalamic Fgf21 did not affect body weight or food intake (Figures S4H and S4I). However, fat mass gain was significantly lower in *Fgf21*$^{fl/fl}$ Tan$^{TAT\text{-}CRE}$ animals than in the control group (Figure 4C). *Fgf21*$^{fl/fl}$ Tan$^{TAT\text{-}CRE}$ mice also showed increased O_2 consumption and energy expenditure (EE) in the dark phase (Figures 4D, 4E, S4J, and S4K), while locomotor activity remained unchanged (Figure S4L). FAO levels (Bruss et al., 2010) also increased during the dark phase (Figure 4F), suggesting that tanycytic Fgf21 deletion altered lipid metabolism.

Tanycytic Fgf21 Deletion Alters Lipid Metabolism in Subcutaneous WAT

We investigated the metabolic effects of tanycytic Fgf21 deletion after fasting. *Fgf21*$^{fl/fl}$ Tan$^{TAT\text{-}CRE}$ mice presented a 25% loss of BAT and subcutaneous (sc)WAT masses compared to control, while liver weight remained unchanged (Figure 4G). scWAT had smaller adipocytes (Figure 4H), revealed by a higher number of adipocytes/mm^2, consistent with a decrease in fat accumulation in Fgf21$^{fl/fl}$ Tan$^{TAT\text{-}CRE}$ mice (Figure S4M). In parallel, we observed a decrease in the expression of lipogenic genes and an increase of the adipose triglyceride lipase gene (*Atgl*; Figure 4I), a critical player in lipolysis (Duncan et al., 2007). *Fgf21*$^{fl/fl}$ Tan$^{TAT\text{-}CRE}$ mice also showed an increase in hormone-sensitive lipase phosphorylation (*Hsl*; Figure 4J), the rate-limiting step in lipolysis (Degerman et al., 1990). Gene expression of the FAO enzyme acetyl-Coa carboxylase 2 (*Acacb*) and of the main browning genes was also increased in *Fgf21*$^{fl/fl}$ Tan$^{TAT\text{-}CRE}$ mice (Figure 4I). Fasted *Fgf21*$^{fl/fl}$ Tan$^{TAT\text{-}CRE}$ mice exhibited higher serum non-esterified fatty acid (NEFA) levels, but no difference in serum glycerol (Figures 4K and 4L), which could be due to a

Figure 3. Determination of the Mechanism of Palmitate-Induced Expression and Secretion of Fgf21 by Tanycytes *In Vitro* and *In Vivo*

(A and B) Time course of Fgf21 expression (A) and secretion (B) upon exposure of cultured tanycytes to palmitate (100 μM).

(C) qRT-PCR analysis of the effect of an i.v. injection of palmitate (100 μM) on the expression levels of *Fgf21* mRNA in medio-basal hypothalamus (ME/MBH) of mice (n = 9/group).

(D) Representative single focal plane fluorescence images showing lipid droplet labeling (BODIPY 493/503) in tanycytes after 2 h of palmitate treatment with or without β-oxidation inhibitor (etomoxir 200 μM) versus control condition (BSA/Eth) *in vitro*.

(E) Oxygen consumption rate measurement in cultured tanycytes after adding palmitate (100 μM, black outline) or BSA/ethanol (gray outline) and etomoxir (200 μM).

(F) Mean OCR at specific time points indicated in (E) (colored arrowheads).

(G) DCF fluorescence emission, as a measure of reactive oxygen species, by cultured tanycytes before and after palmitate treatment.

(H) Mean DCF fluorescence emission by cultured tanycytes treated with palmitate in presence or absence of a ROS inhibitor (NAC, 1 mM).

(I) qRT-PCR analysis of the effect of palmitate treatment for 6 h with or without NAC on the expression level of *Fgf21* mRNA in cultured tanycytes.

(J and K) Representative western blots (left panel) and quantitative comparison (right panel) of phosphorylated and total p38-MAPK in cultured tanycytes after palmitate treatment as a function of time (J) or after 6 h of palmitate treatment with or without NAC (K).

(L and M) Effect of palmitate and the p38-MAPK inhibitor (SB203580, 10 μM) on the expression level of *Fgf21* mRNA (L) and Fgf21 secretion (M) by cultured tanycytes.

(N) qRT-PCR analysis of the effect of an i.v injection of palmitate (100 μM) and an intracerebroventricular injection of a p38-MAPK inhibitor (SB203580) on the expression level of *Fgf21* mRNA in the ME (n = 5–8 per group).

(O) Proposed schematic of the signaling pathway activated by palmitate to induce Fgf21 in tanycytes. Scale bars, 50 μm (D and G). For multiple comparisons with the control, one-way ANOVA followed by Dunnett's test was performed. For simple comparison, unpaired t tests were performed. *p < 0.05; **p < 0.01; ***p < 0.001; ****p < 0.0001. Values indicate means ± SEM. See also Figure S4.

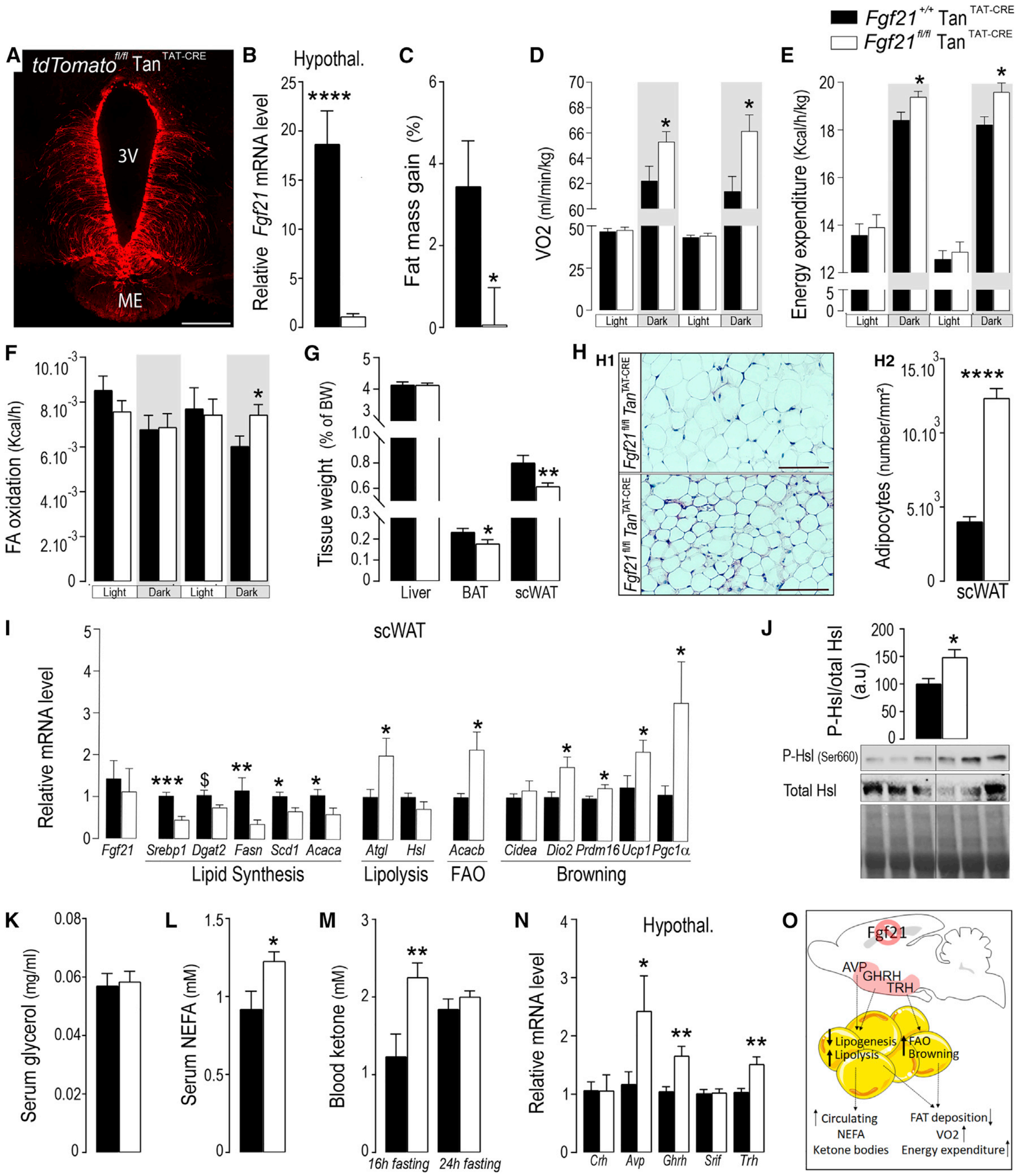

Figure 4. Impact of Tanycytic Fgf21 Deletion on Energy Balance and Lipid Metabolism

(A) Representative photomicrograph showing tdTomato production by tanycytes after TAT-CRE injection in 3V of tdTomato$^{fl/fl}$ mice.

(B–N) Effect of tanycytic Fgf21 deletion on (B) hypothalamic *Fgf21* mRNA expression (n = 17–18), (C) percent (%) body fat mass gain change (n = 7), (D) oxygen consumption (VO_2), (E) energy expenditure, and (F) whole-body fatty acid oxidation during light and dark phases (n = 5–7).

(G) Liver, BAT, and scWAT masses expressed as percent (%) body weight (n = 10–11).

(H) scWAT histology stained with H&E (H1) and the number of adipocytes per mm^2 (H2) (n = 10–11).

(I) Expression levels of genes promoting lipogenesis, lipolysis, fatty acid oxidation (FAO), and browning in scWAT (n = 6).

(J) Ser660 phosphorylation of Hsl (n = 10–11).

(K and L) Serum levels of glycerol (K) and NEFA (L) after 16 h of fasting (n = 10–11).

(M) Blood levels of ketone bodies after 16 and 24 h of fasting (n = 3–4 and 6–7, respectively).

(N) mRNA expression of hypothalamic neuropeptides involved in lipid metabolism regulation (n = 6–7 for Crh and Srif and n = 17–18 for Avp, Ghrh, and Trh).

(O) Proposed schematic of lipid metabolism regulation by tanycytic Fgf21 and downstream hypothalamic pathways. n indicates the number of animals per group. Scale bars, 200 μm (A) and 100 μm (H1). Unpaired t tests or Mann-Whitney tests were performed. *p < 0.05; **p < 0.01; ***p < 0.001; ****p < 0.001; $p = 0.07. Values indicate means ± SEM. See also Figure S4.

more rapid increase of serum NEFAs than serum glycerol (Sim et al., 1964). Fgf21$^{fl/fl}$ Tan$^{TAT-CRE}$ mice also presented a higher blood ketonemia (Figures 4M and S4N). These data suggest that tanycytic Fgf21 deletion promotes lipid mobilization from scWAT, increasing ketone bodies production by the liver, and an scWAT browning, resulting in an increase in EE and a decrease in fat accumulation (Figure 4O).

Lipolysis in WAT is regulated by hormones and by the sympathetic nervous system (SNS). These two systems are controlled by hypothalamic neurons, such as arginine-vasopressin (Avp), corticotrophin-releasing hormone (Crh), thyrotropin-releasing hormone (Trh), growth-hormone-releasing hormone (Ghrh), or somatostatin (Srif) neurons. Fgf21 was shown to act centrally and to regulate the HPA axis and sympathetic activity (Bookout et al., 2013; Owen et al., 2014; Recinella et al., 2017). We hypothesize that tanycytic Fgf21 could regulate WAT lipolysis through a paracrine action on these hypothalamic neurons. Indeed, *Fgf21$^{fl/fl}$* Tan$^{TAT-CRE}$ mice exhibited higher hypothalamic expression of *Avp*, *Ghrh*, and *Trh* mRNAs (Figure 4N). Trh and Crh neurons are known to promote cellular metabolism, EE, and browning of WAT (Contreras et al., 2016; Münzberg et al., 2016). Ghrh and Avp neurons have been shown to promote the utilization of lipids, to induce a decrease in fat accumulation, to increase fat mobilization from WAT, and to increase hepatic FFA uptake (Fernández-Pérez et al., 2013; Mavani et al., 2015).

Tanycytic Fgf21 Deletion Alters Glucose Homeostasis

Fgf21$^{fl/fl}$ Tan$^{tat-cre}$ mice presented a higher hepatic expression of *Igf-1* and of *de novo* lipid synthesis genes (Figure S4P), consistent with an activation of the hypothalamic-pituitary-somatotropic (HPS) axis by Ghrh (Fernández-Pérez et al., 2013). However, after fasting, we did not observe an increased accumulation of lipids in *Fgf21$^{fl/fl}$* Tan$^{TAT-CRE}$ livers (arrows, Figure S4P). *Fgf21$^{fl/fl}$* Tan$^{TAT-CRE}$ mice had a higher glycemia after 24 h of fasting and higher blood glucose levels after pyruvate (PTT) or glucose (GTT) intraperitoneal injection (Figures S4Q–S4S), suggesting a higher capacity to produce glucose and/or a difficulty to regulate glycemia. Avp and Ghrh are also involved in the maintenance of glucose homeostasis by regulating (1) glucose production by the liver or the kidney, (2) insulin signaling, and (3) body fluids and glucagon production. Pancreatic Fgf21 was recently shown to regulate insulin production (Pan et al., 2019). However, *Fgf21$^{fl/fl}$* Tan$^{tat-cre}$ mice did not show abnormal insulin levels (Figure S4T) after fasting (T0) or glucose injection (T20). Serum levels of glucagon, a primary regulator of hepatic glucose production, lipolysis, ketogenesis, and EE, were not altered 24 h post-fasting (Figure S4U). During Ghrh-induced Gh hypersecretion, the increase of WAT-produced FFAs can induce hepatic and/or systemic insulin resistance and glucose metabolism alterations (Mavani et al., 2015; Vijayakumar et al., 2010). The quantitative insulin sensitivity check index (QUICKI) (Berglund et al., 2008) revealed a tendency of *Fgf21$^{fl/fl}$* Tan$^{TAT-CRE}$ mice to be less sensitive to insulin (Figure S4V). These data suggest that an increase of fat mobilization from scWAT in tanycytic Fgf21-knockout (KO) mice induces hepatic *de novo* lipid synthesis and hyperglycemia (Figure S4W).

Fasting, via circulating FFAs, induces tanycytic Fgf21 production and secretion. FFAs have been shown to downregulate HPA and HPS axis activation by blocking Avp and Ghrh production, without any effect on Crh production (Casanueva et al., 1987; Oh et al., 2012). FFAs cause a decrease in Tsh and T3/T4 levels, thus inhibiting Trh production (Vermaak et al., 1986), and inhibit the SNS by reducing sympathetic nerve activity (SNA) and plasma norepinephrine concentration (Magnan et al., 2001; Migrenne et al., 2011). A negative energy balance in animals and humans consistently inhibits the HPT and HPS axes by inhibiting *Trh* and *Ghrh* hypothalamic expression (Boelen et al., 2008; Carro et al., 1999; Park et al., 2004). The absence of tanycytic Fgf21 production would prevent the inhibition of these neurons by fasting and/or FFAs. We propose that, upon fasting and/or palmitate stimulation, tanycytic Fgf21 inhibits *Ghrh*, *Avp*, and *Trh* expression, inhibiting lipolysis and promoting lipogenesis in scWAT (Figures 4O and S4W).

Hypothalamic Fgf21 Is a Key Factor Participating in the Maintenance of Whole-Body Energy Homeostasis

Trh, Avp, and Ghrh neurons are located in the PVN, SCN, and ARC, respectively. Fgfr1 and Klb are detected in these hypothalamic areas. Mice overexpressing Fgf21 (Fgf21-Tg) have a low expression of Avp, while mice lacking hypothalamic Klb (Klb$^{tm1(camk2a)}$) have a higher expression of *Avp* (Bookout et al., 2013). These observations agree with our increase of *Avp* expression in the absence of hypothalamic Fgf21. An action of Fgf21 on Trh neurons was recently proposed, but unlike our data, chronic brain infusion of Fgf21 increased *Trh* expression in rats (Yilmaz et al., 2018). However, high levels of Fgf21 detected in patients with hypothyroidism and low TH levels observed after Fgf21 administration in rodents (Domouzoglou et al., 2014; Lee et al., 2013) can be explained by our results since we show that Fgf21 inhibits Trh neurons. It was shown in Fgf21-Tg mice that Fgf21 represses the Gh/Igf-1 axis in liver (Zhang et al., 2012). Our study suggests an additional direct hypothalamic action of Fgf21 on the HPS axis. The similarities in phenotype between Fgf21-Tg mice and Ghrh-KO mice concerning growth or lifespan also support a negative regulation of Ghrh neurons by Fgf21 (Bookout et al., 2013; Satoh and Imai, 2014). It was proposed that the inhibition of the HPS axis by Fgf21 aims to preserve energy under starvation conditions due to its negative effect on growth (Zhang et al., 2012). Fgf21 was also shown to reduce overall activity and inhibit female fertility (Bookout et al., 2013; Owen et al., 2013). These phenotypes constitute an adaptive starvation response and involve a neuroendocrine control (Sainsbury and Zhang, 2012). Our study supports this hypothesis by showing that tanycytic Fgf21 deletion increases EE and reduces accumulation of body fat. We propose that central Fgf21 acts (either directly or indirectly) on Avp, Ghrh, and Trh neurons to reduce EE and to promote lipid accumulation in WAT, two processes induced by a negative energy balance to preserve energy (Sainsbury and Zhang, 2012). Specific deletion of *Klb* will need to be done to determine the direct implication of these neurons in tanycytic Fgf21 function.

The effects of Fgf21 on energy metabolism are still controversial (Solon-Biet et al., 2016; Zhang et al., 2015). In obesity, systemic administration and transgenic overexpression of Fgf21 led to enhanced insulin sensitivity by a direct action on adipose tissue but also induced weight loss and increased EE by acting on the brain and inducing a sympathetic stimulation of WAT and BAT (Coskun et al., 2008; Kharitonenkov et al., 2005; Lin et al., 2017; Owen et al., 2014; Sarruf et al., 2010; Véniant et al., 2012). In lean rodents, chronic Fgf21 infusion or overall transgenic overexpression led to weight loss and decreased body fat content by acting on the brain, but not on adipose tissue; increased O_2 consumption and browning of WAT by acting amongst others on the brain; increased food intake without a central action; and finally, increased serum FFAs by inducing lipolysis in WAT (Douris et al., 2015; Fisher et al., 2012; Inagaki et al., 2007; Véniant et al., 2015; Yilmaz et al., 2018). We investigated the role of tanycyte-secreted Fgf21 in the context of fasting in lean rodents and focused on the short-term effects of Fgf21 deletion on lipid metabolism. The contradictory results observed between these studies and ours could be due to differences in the metabolic status of animals (obese versus lean or fed versus fast), Fgf21 action (chronic versus acute), and direct action or adaptive consequences of Fgf21 deletion (developmental versus inducible models). It was previously shown, using Fgf21 KO mice, that Fgf21 stimulates WAT lipolysis in feeding but inhibits it in fasting (Hotta et al., 2009). It was also shown that overexpression of *Fgf21* in hypertriglyceridemic mice suppressed WAT lipolysis and improved hepatic steatosis after fasting (Park et al., 2016). However, direct effects of Fgf21 on adipose tissue lipolysis led to contradictory results using *ex vivo* and *in vitro* models of adipocytes (Arner et al., 2008; Inagaki et al., 2007; Park et al., 2016). Our study suggests that tanycyte-produced Fgf21 inhibits lipolysis during fasting by acting, at least in part, centrally through key hypothalamic neuronal populations, acting as a negative feedback loop to maintain homeostatic levels of circulating FFAs.

The use of lean *Fgf21*-deleted mice (*Fgf21*-KO and *Fgf21* liver KO) or *Fgfr1* WAT KO mice has shown that Fgf21 limits lipotoxicity by reducing circulating FFAs and hepatic FA accumulation (Badman et al., 2007; Fisher et al., 2014; Yang et al., 2012). Recently, it was proposed that Fgf21-dependent improvement in serum FFAs and hepatic steatosis relies on a direct brain Fgf21 signaling (Benedini and Luzi, 2016; Nies et al., 2015). Our study supports this view, as we show that Fgf21 acts centrally to regulate lipid metabolism in scWAT and liver. By reducing scWAT lipolysis and hepatic lipogenesis, tanycytic Fgf21 limits lipotoxicity. Hepatic *Fgf21* deletion caused fatty liver but did not trigger changes in *de novo* lipogenesis genes, unlike in *Fgf21*-KO mice (Badman et al., 2007), suggesting an alternative mechanism that does not require hepatic Fgf21. Our results suggest an endocrine regulation of hepatic lipogenesis by tanycytic Fgf21 through the HPS axis. All these results suggest that hepatic and tanycytic Fgf21 limit lipotoxicity by different mechanisms. The long-term effects of tanycytic Fgf21 deletion on liver metabolism under chow, high-fat, and ketogenic diet conditions need to be determined.

Limitations of Study

We show that tanycytic *Fgf21* expression in the hypothalamus is triggered in response to circulating FFAs; however, the weak expression of this hypothalamic *Fgf21* constitutes a limit for the identification of conditions inducing its down-regulation. The strategy to study the physiological role of tanycytic Fgf21, using TAT-CRE and $Fgf21^{fl/fl}$ mice, may allow for a residual expression of Fgf21, which could in turn minimize the phenotype observed. We can also not exclude the existence of a compensation system inducing a modification in Fgf21 production in other peripheral tissues than scWAT and liver (already tested) that could also modulate the phenotype. In addition, we have collected physiological data using indirect calorimetry on a small sample size (n = 5–7), which could curtail the differences observed between both groups. We used $Fgf21^{+/+}$ mice as a control to exclude any indirect effects of the TAT-CRE. $Fgf21^{+/+}$ mice and $Fgf21^{fl/fl}$ mice possess the same genetic background, but to avoid the question of the possible physiologic impact of Fgf21-LoxP construct, we performed additional metabolic phenotyping in all mice prior to TAT-CRE injection.

STAR★METHODS

Detailed methods are provided in the online version of this paper and include the following:

- KEY RESOURCES TABLE
- LEAD CONTACT AND MATERIALS AVAILABILITY
- EXPERIMENTAL MODEL AND SUBJECT DETAILS
  - Animals
  - Fasting Test
  - Treatment Protocols and Stereotaxic Surgery
  - Physiological Measurements
  - Cell Culture
- METHOD DETAILS
  - Brain, Liver and scWAT Sample Processing
  - RNA and Protein Purification
  - RT-PCR and Plasmid Cloning
  - RT-qPCR
  - Fgf21 ELISA Measurement
  - ROS-Oxidized DCF Measurement
  - *In Situ* Hybridization
  - Immunofluorescence
  - Hematoxylin and Eosin Staining
  - Western Blot Analysis
  - Seahorse Analysis
- QUANTIFICATION AND STATISTICAL ANALYSIS

SUPPLEMENTAL INFORMATION

Supplemental Information can be found online at https://doi.org/10.1016/j.cmet.2019.08.004.

ACKNOWLEDGMENTS

We thank Dr. Stehle of the Mouse Pathology Facility for histological processing, Pr. Pitteloud and Dr. Somm for providing $Fgf21^{-/-}$ and $Klb^{-/-}$ mice, Pr. Fajas Coll and Dr. Nasrallah for 3T3-L1 cells, and Dr. Prévot for GnRH-GFP brain samples. This work was supported by SNF grants (no. 31003A-140957 to L.P., no. 320030_170062 to F.A., Sinergia grant CRSII3_141960 to L.P., and Ambizione PZ00P3_168077 to I.C.L.-M.). L.P. received financial support for this project from the Department of Physiology, University of Lausanne and from the program IdEx Bordeaux ANR-10-IDEX-03-02.

AUTHOR CONTRIBUTIONS

Conceptualization, S.G.; Methodology, S.G., Y.A., S.L., and I.C.L.-M.; Investigation, S.G. performed all the experiments with the help of Y.A., C.N., S.L., L.C., and I.C.L.-M.; L.Z. performed i.v. injections; Formal Analysis, S.G., Y.A., S.L., and I.C.L.-M.; Writing – Original Draft, S.G.; Writing – Review & Editing, S.G., Y.A., S.L., L.Z., F.A., I.C.L.-M., and L.P.; Project Administration, S.G.; Funding Acquisition and Resources, F.A., I.C.L.-M., and L.P.; Project Supervision, L.P.

DECLARATION OF INTERESTS

The authors declare no competing interests.

Received: January 17, 2018
Revised: December 28, 2018
Accepted: August 5, 2019
Published: August 29, 2019

REFERENCES

Allaman, I., Gavillet, M., Bélanger, M., Laroche, T., Viertl, D., Lashuel, H.A., and Magistretti, P.J. (2010). Amyloid-beta aggregates cause alterations of astrocytic metabolic phenotype: impact on neuronal viability. J. Neurosci. *30*, 3326–3338.

Arner, P., Pettersson, A., Mitchell, P.J., Dunbar, J.D., Kharitonenkov, A., and Rydén, M. (2008). FGF21 attenuates lipolysis in human adipocytes - a possible link to improved insulin sensitivity. FEBS Lett. *582*, 1725–1730.

Badman, M.K., Pissios, P., Kennedy, A.R., Koukos, G., Flier, J.S., and Maratos-Flier, E. (2007). Hepatic fibroblast growth factor 21 is regulated by PPARalpha and is a key mediator of hepatic lipid metabolism in ketotic states. Cell Metab. *5*, 426–437.

Balland, E., Dam, J., Langlet, F., Caron, E., Steculorum, S., Messina, A., Rasika, S., Falluel-Morel, A., Anouar, Y., Dehouck, B., et al. (2014). Hypothalamic tanycytes are an ERK-gated conduit for leptin into the brain. Cell Metab. *19*, 293–301.

Benedini, S., and Luzi, L. (2016). Lipodystrophy HIV-related and FGF21: a new marker to follow the progression of lipodystrophy? J. Transl. Int. Med. *4*, 150–154.

Berglund, E.D., Li, C.Y., Poffenberger, G., Ayala, J.E., Fueger, P.T., Willis, S.E., Jewell, M.M., Powers, A.C., and Wasserman, D.H. (2008). Glucose metabolism in vivo in four commonly used inbred mouse strains. Diabetes *57*, 1790–1799.

Boelen, A., Wiersinga, W.M., and Fliers, E. (2008). Fasting-induced changes in the hypothalamus-pituitary-thyroid axis. Thyroid *18*, 123–129.

Bookout, A.L., de Groot, M.H., Owen, B.M., Lee, S., Gautron, L., Lawrence, H.L., Ding, X., Elmquist, J.K., Takahashi, J.S., Mangelsdorf, D.J., et al. (2013). FGF21 regulates metabolism and circadian behavior by acting on the nervous system. Nat. Med. *19*, 1147–1152.

Bruss, M.D., Khambatta, C.F., Ruby, M.A., Aggarwal, I., and Hellerstein, M.K. (2010). Calorie restriction increases fatty acid synthesis and whole body fat oxidation rates. Am. J. Physiol. Endocrinol. Metab. *298*, E108–E116.

Carneiro, L., Geller, S., Fioramonti, X., Hébert, A., Repond, C., Leloup, C., and Pellerin, L. (2016). Evidence for hypothalamic ketone body sensing: impact on food intake and peripheral metabolic responses in mice. Am. J. Physiol. Endocrinol. Metab. *310*, E103–E115.

Carneiro, L., Asrih, M., Repond, C., Sempoux, C., Stehle, J.C., Leloup, C., Jornayvaz, F.R., and Pellerin, L. (2017). AMPK activation caused by reduced liver lactate metabolism protects against hepatic steatosis in MCT1 haploinsufficient mice. Mol. Metab. *6*, 1625–1633.

Carro, E., Señarís, R.M., Seoane, L.M., Frohman, L.A., Arimura, A., Casanueva, F.F., and Diéguez, C. (1999). Role of growth hormone (GH)-releasing hormone and somatostatin on leptin-induced GH secretion. Neuroendocrinology *69*, 3–10.

Casanueva, F.F., Villanueva, L., Dieguez, C., Diaz, Y., Cabranes, J.A., Szoke, B., Scanlon, M.F., Schally, A.V., and Fernandez-Cruz, A. (1987). Free fatty acids block growth hormone (GH) releasing hormone-stimulated GH secretion in man directly at the pituitary. J. Clin. Endocrinol. Metab. *65*, 634–642.

Contreras, C., Nogueiras, R., Diéguez, C., Medina-Gómez, G., and López, M. (2016). Hypothalamus and thermogenesis: heating the BAT, browning the WAT. Mol. Cell. Endocrinol. *438*, 107–115.

Coskun, T., Bina, H.A., Schneider, M.A., Dunbar, J.D., Hu, C.C., Chen, Y., Moller, D.E., and Kharitonenkov, A. (2008). Fibroblast growth factor 21 corrects obesity in mice. Endocrinology *149*, 6018–6027.

Degerman, E., Smith, C.J., Tornqvist, H., Vasta, V., Belfrage, P., and Manganiello, V.C. (1990). Evidence that insulin and isoprenaline activate the cGMP-inhibited low-Km cAMP phosphodiesterase in rat fat cells by phosphorylation. Proc. Natl. Acad. Sci. USA *87*, 533–537.

Domouzoglou, E.M., Fisher, F.M., Astapova, I., Fox, E.C., Kharitonenkov, A., Flier, J.S., Hollenberg, A.N., and Maratos-Flier, E. (2014). Fibroblast growth factor 21 and thyroid hormone show mutual regulatory dependency but have independent actions in vivo. Endocrinology *155*, 2031–2040.

Douris, N., Stevanovic, D.M., Fisher, F.M., Cisu, T.I., Chee, M.J., Nguyen, N.L., Zarebidaki, E., Adams, A.C., Kharitonenkov, A., Flier, J.S., et al. (2015). Central fibroblast growth factor 21 browns white fat via sympathetic action in male mice. Endocrinology *156*, 2470–2481.

Drougard, A., Fournel, A., Valet, P., and Knauf, C. (2015). Impact of hypothalamic reactive oxygen species in the regulation of energy metabolism and food intake. Front. Neurosci. *9*, 56.

Duncan, R.E., Ahmadian, M., Jaworski, K., Sarkadi-Nagy, E., and Sul, H.S. (2007). Regulation of lipolysis in adipocytes. Annu. Rev. Nutr. *27*, 79–101.

Fernández-Pérez, L., Guerra, B., Díaz-Chico, J.C., and Flores-Morales, A. (2013). Estrogens regulate the hepatic effects of growth hormone, a hormonal interplay with multiple fates. Front. Endocrinol. (Lausanne) *4*, 66.

Fisher, F.M., Kleiner, S., Douris, N., Fox, E.C., Mepani, R.J., Verdeguer, F., Wu, J., Kharitonenkov, A., Flier, J.S., Maratos-Flier, E., et al. (2012). FGF21 regulates PGC-1alpha and browning of white adipose tissues in adaptive thermogenesis. Genes Dev. *26*, 271–281.

Fisher, F.M., Chui, P.C., Nasser, I.A., Popov, Y., Cunniff, J.C., Lundasen, T., Kharitonenkov, A., Schuppan, D., Flier, J.S., and Maratos-Flier, E. (2014). Fibroblast growth factor 21 limits lipotoxicity by promoting hepatic fatty acid activation in mice on methionine and choline-deficient diets. Gastroenterology *147*, 1073–1083.e6.

Fon Tacer, K., Bookout, A.L., Ding, X., Kurosu, H., John, G.B., Wang, L., Goetz, R., Mohammadi, M., Kuro-o, M., Mangelsdorf, D.J., et al. (2010). Research resource: comprehensive expression atlas of the fibroblast growth factor system in adult mouse. Mol. Endocrinol *24*, 2050–2064.

Geller, S., Lomet, D., Caraty, A., Tillet, Y., Duittoz, A., and Vaudin, P. (2017). Rostro-caudal maturation of glial cells in the accessory olfactory system during development: involvement in outgrowth of GnRH neurites. Eur. J. Neurosci. *46*, 2596–2607.

Guan, D., Zhao, L., Chen, D., Yu, B., and Yu, J. (2016). Regulation of fibroblast growth factor 15/19 and 21 on metabolism: in the fed or fasted state. J. Transl. Med. *14*, 63.

Hotta, Y., Nakamura, H., Konishi, M., Murata, Y., Takagi, H., Matsumura, S., Inoue, K., Fushiki, T., and Itoh, N. (2009). Fibroblast growth factor 21 regulates lipolysis in white adipose tissue but is not required for ketogenesis and triglyceride clearance in liver. Endocrinology *150*, 4625–4633.

Hsuchou, H., Pan, W., and Kastin, A.J. (2007). The fasting polypeptide FGF21 can enter brain from blood. Peptides *28*, 2382–2386.

Inagaki, T., Dutchak, P., Zhao, G., Ding, X., Gautron, L., Parameswara, V., Li, Y., Goetz, R., Mohammadi, M., Esser, V., et al. (2007). Endocrine regulation of the fasting response by PPARalpha-mediated induction of fibroblast growth factor 21. Cell Metab. *5*, 415–425.

Ito, S., Fujimori, T., Furuya, A., Satoh, J., Nabeshima, Y., and Nabeshima, Y. (2005). Impaired negative feedback suppression of bile acid synthesis in mice lacking betaKlotho. J. Clin. Invest. *115*, 2202–2208.

Jeanson, Y., Ribas, F., Galinier, A., Arnaud, E., Ducos, M., André, M., Chenouard, V., Villarroya, F., Casteilla, L., and Carrière, A. (2016). Lactate induces FGF21 expression in adipocytes through a p38-MAPK pathway. Biochem. J. *473*, 685–692.

Jensen, M.D., Haymond, M.W., Gerich, J.E., Cryer, P.E., and Miles, J.M. (1987). Lipolysis during fasting. Decreased suppression by insulin and increased stimulation by epinephrine. J. Clin. Invest. *79*, 207–213.

Karmi, A., Iozzo, P., Viljanen, A., Hirvonen, J., Fielding, B.A., Virtanen, K., Oikonen, V., Kemppainen, J., Viljanen, T., Guiducci, L., et al. (2010). Increased brain fatty acid uptake in metabolic syndrome. Diabetes *59*, 2171–2177.

Kharitonenkov, A., Shiyanova, T.L., Koester, A., Ford, A.M., Micanovic, R., Galbreath, E.J., Sandusky, G.E., Hammond, L.J., Moyers, J.S., Owens, R.A., et al. (2005). FGF-21 as a novel metabolic regulator. J. Clin. Invest. *115*, 1627–1635.

Kokorovic, A., Cheung, G.W., Rossetti, L., and Lam, T.K. (2009). Hypothalamic sensing of circulating lactate regulates glucose production. J. Cell. Mol. Med. *13*, 4403–4408.

Lagarrigue, S., Lopez-Mejia, I.C., Denechaud, P.D., Escoté, X., Castillo-Armengol, J., Jimenez, V., Chavey, C., Giralt, A., Lai, Q., Zhang, L., et al. (2016). CDK4 is an essential insulin effector in adipocytes. J. Clin. Invest. *126*, 335–348.

Langlet, F., Levin, B.E., Luquet, S., Mazzone, M., Messina, A., Dunn-Meynell, A.A., Balland, E., Lacombe, A., Mazur, D., Carmeliet, P., et al. (2013). Tanycytic VEGF-A boosts blood-hypothalamus barrier plasticity and access of metabolic signals to the arcuate nucleus in response to fasting. Cell Metab. *17*, 607–617.

Le Foll, C., and Levin, B.E. (2016). Fatty acid-induced astrocyte ketone production and the control of food intake. Am. J. Physiol. Regul. Integr. Comp. Physiol. *310*, R1186–R1192.

Lee, Y., Park, Y.J., Ahn, H.Y., Lim, J.A., Park, K.U., Choi, S.H., Park, D.J., Oh, B.C., Jang, H.C., and Yi, K.H. (2013). Plasma FGF21 levels are increased in patients with hypothyroidism independently of lipid profile. Endocr. J. *60*, 977–983.

Leloup, C., Allard, C., Carneiro, L., Fioramonti, X., Collins, S., and Pénicaud, L. (2016). Glucose and hypothalamic astrocytes: more than a fueling role? Neuroscience *323*, 110–120.

Liang, F., Hatanaka, Y., Saito, H., Yamamori, T., and Hashikawa, T. (2000). Differential expression of gamma-aminobutyric acid type B receptor-1a and -1b mRNA variants in GABA and non-GABAergic neurons of the rat brain. J. Comp. Neurol. *416*, 475–495.

Liang, Q., Zhong, L., Zhang, J., Wang, Y., Bornstein, S.R., Triggle, C.R., Ding, H., Lam, K.S., and Xu, A. (2014). FGF21 maintains glucose homeostasis by mediating the cross talk between liver and brain during prolonged fasting. Diabetes *63*, 4064–4075.

Lin, X., Liu, Y.B., and Hu, H. (2017). Metabolic role of fibroblast growth factor 21 in liver, adipose and nervous system tissues. Biomed. Rep. *6*, 495–502.

Lopez-Mejia, I.C., Lagarrigue, S., Giralt, A., Martinez-Carreres, L., Zanou, N., Denechaud, P.D., Castillo-Armengol, J., Chavey, C., Orpinell, M., Delacuisine, B., et al. (2017). CDK4 phosphorylates AMPKalpha2 to inhibit its activity and repress fatty acid oxidation. Mol. Cell *68*, 336–349.e6.

Ly, L.D., Xu, S., Choi, S.K., Ha, C.M., Thoudam, T., Cha, S.K., Wiederkehr, A., Wollheim, C.B., Lee, I.K., and Park, K.S. (2017). Oxidative stress and calcium dysregulation by palmitate in type 2 diabetes. Exp. Mol. Med. *49*, e291.

Madisen, L., Zwingman, T.A., Sunkin, S.M., Oh, S.W., Zariwala, H.A., Gu, H., Ng, L.L., Palmiter, R.D., Hawrylycz, M.J., Jones, A.R., et al. (2010). A robust and high-throughput Cre reporting and characterization system for the whole mouse brain. Nat. Neurosci. *13*, 133–140.

Magnan, C., Cruciani, C., Clément, L., Adnot, P., Vincent, M., Kergoat, M., Girard, A., Elghozi, J.L., Velho, G., Beressi, N., et al. (2001). Glucose-induced insulin hypersecretion in lipid-infused healthy subjects is associated with a decrease in plasma norepinephrine concentration and urinary excretion. J. Clin. Endocrinol. Metab. *86*, 4901–4907.

Mäkelä, J., Tselykh, T.V., Maiorana, F., Eriksson, O., Do, H.T., Mudò, G., Korhonen, L.T., Belluardo, N., and Lindholm, D. (2014). Fibroblast growth factor-21 enhances mitochondrial functions and increases the activity of PGC-1alpha in human dopaminergic neurons via Sirtuin-1. Springerplus *3*, 2.

Markan, K.R., Naber, M.C., Ameka, M.K., Anderegg, M.D., Mangelsdorf, D.J., Kliewer, S.A., Mohammadi, M., and Potthoff, M.J. (2014). Circulating FGF21 is liver derived and enhances glucose uptake during refeeding and overfeeding. Diabetes *63*, 4057–4063.

Mavani, G.P., DeVita, M.V., and Michelis, M.F. (2015). A review of the nonpressor and nonantidiuretic actions of the hormone vasopressin. Front. Med. (Lausanne) *2*, 19.

Migrenne, S., Le Foll, C., Levin, B.E., and Magnan, C. (2011). Brain lipid sensing and nervous control of energy balance. Diabetes Metab. *37*, 83–88.

Münzberg, H., Qualls-Creekmore, E., Berthoud, H.R., Morrison, C.D., and Yu, S. (2016). Neural control of energy expenditure. Handb. Exp. Pharmacol. *233*, 173–194.

Nies, V.J., Sancar, G., Liu, W., van Zutphen, T., Struik, D., Yu, R.T., Atkins, A.R., Evans, R.M., Jonker, J.W., and Downes, M.R. (2015). Fibroblast growth factor signaling in metabolic regulation. Front. Endocrinol. (Lausanne) *6*, 193.

Oh, Y.T., Oh, K.S., Kang, I., and Youn, J.H. (2012). A fall in plasma free fatty acid (FFA) level activates the hypothalamic-pituitary-adrenal axis independent of plasma glucose: evidence for brain sensing of circulating FFA. Endocrinology *153*, 3587–3592.

Owen, B.M., Bookout, A.L., Ding, X., Lin, V.Y., Atkin, S.D., Gautron, L., Kliewer, S.A., and Mangelsdorf, D.J. (2013). FGF21 contributes to neuroendocrine control of female reproduction. Nat. Med. *19*, 1153–1156.

Owen, B.M., Ding, X., Morgan, D.A., Coate, K.C., Bookout, A.L., Rahmouni, K., Kliewer, S.A., and Mangelsdorf, D.J. (2014). FGF21 acts centrally to induce sympathetic nerve activity, energy expenditure, and weight loss. Cell Metab. *20*, 670–677.

Pan, J.W., Rothman, T.L., Behar, K.L., Stein, D.T., and Hetherington, H.P. (2000). Human brain beta-hydroxybutyrate and lactate increase in fasting-induced ketosis. J. Cereb. Blood Flow Metab. *20*, 1502–1507.

Pan, Y., Wang, B., Zheng, J., Xiong, R., Fan, Z., Ye, Y., Zhang, S., Li, Q., Gong, F., Wu, C., et al. (2019). Pancreatic fibroblast growth factor 21 protects against type 2 diabetes in mice by promoting insulin expression and secretion in a PI3K/Akt signaling-dependent manner. J. Cell. Mol. Med. *23*, 1059–1071.

Park, S., Sohn, S., and Kineman, R.D. (2004). Fasting-induced changes in the hypothalamic-pituitary-GH axis in the absence of GH expression: lessons from the spontaneous dwarf rat. J. Endocrinol. *180*, 369–378.

Park, J.G., Xu, X., Cho, S., Hur, K.Y., Lee, M.S., Kersten, S., and Lee, A.H. (2016). CREBH-FGF21 axis improves hepatic steatosis by suppressing adipose tissue lipolysis. Sci. Rep. *6*, 27938.

Petryszak, R., Keays, M., Tang, Y.A., Fonseca, N.A., Barrera, E., Burdett, T., Füllgrabe, A., Fuentes, A.M., Jupp, S., Koskinen, S., et al. (2016). Expression Atlas update–an integrated database of gene and protein expression in humans, animals and plants. Nucleic Acids Res. *44*, D746–D752.

Pinto, S., Roseberry, A.G., Liu, H., Diano, S., Shanabrough, M., Cai, X., Friedman, J.M., and Horvath, T.L. (2004). Rapid rewiring of arcuate nucleus feeding circuits by leptin. Science *304*, 110–115.

Potthoff, M.J., Inagaki, T., Satapati, S., Ding, X., He, T., Goetz, R., Mohammadi, M., Finck, B.N., Mangelsdorf, D.J., Kliewer, S.A., et al. (2009). FGF21 induces PGC-1alpha and regulates carbohydrate and fatty acid metabolism during the adaptive starvation response. Proc. Natl. Acad. Sci. USA *106*, 10853–10858.

Prevot, V., Rio, C., Cho, G.J., Lomniczi, A., Heger, S., Neville, C.M., Rosenthal, N.A., Ojeda, S.R., and Corfas, G. (2003). Normal female sexual development requires neuregulin-erbB receptor signaling in hypothalamic astrocytes. J. Neurosci. *23*, 230–239.

Recinella, L., Leone, S., Ferrante, C., Chiavaroli, A., Di Nisio, C., Martinotti, S., Vacca, M., Brunetti, L., and Orlando, G. (2017). Effects of central fibroblast growth factor 21 (FGF21) in energy balance. J. Biol. Regul. Homeost. Agents *31*, 603–613.

Restelli, L.M., Oettinghaus, B., Halliday, M., Agca, C., Licci, M., Sironi, L., Savoia, C., Hench, J., Tolnay, M., Neutzner, A., et al. (2018). Neuronal mitochondrial dysfunction activates the integrated stress response to induce fibroblast growth factor 21. Cell Rep. *24*, 1407–1414.

Ribas, F., Villarroya, J., Hondares, E., Giralt, M., and Villarroya, F. (2014). FGF21 expression and release in muscle cells: involvement of MyoD and regulation by mitochondria-driven signalling. Biochem. J. *463*, 191–199.

Sainsbury, A., and Zhang, L. (2012). Role of the hypothalamus in the neuroendocrine regulation of body weight and composition during energy deficit. Obes. Rev. *13*, 234–257.

Sa-Nguanmoo, P., Chattipakorn, N., and Chattipakorn, S.C. (2016). Potential roles of fibroblast growth factor 21 in the brain. Metab. Brain Dis. *31*, 239–248.

Sarruf, D.A., Thaler, J.P., Morton, G.J., German, J., Fischer, J.D., Ogimoto, K., and Schwartz, M.W. (2010). Fibroblast growth factor 21 action in the brain increases energy expenditure and insulin sensitivity in obese rats. Diabetes *59*, 1817–1824.

Satoh, A., and Imai, S. (2014). Systemic regulation of mammalian ageing and longevity by brain sirtuins. Nat. Commun. *5*, 4211.

Schneider, C.A., Rasband, W.S., and Eliceiri, K.W. (2012). NIH Image to ImageJ: 25 years of image analysis. Nat. Methods *9*, 671–675.

Sim, A.W., de Vries, J.W., and Vincent, J.E. (1964). Concentrations of glycerol and non-esterified fatty acids in plasma during fat mobilization. Biochem. J. *92*, 590–593.

Solon-Biet, S.M., Cogger, V.C., Pulpitel, T., Heblinski, M., Wahl, D., McMahon, A.C., Warren, A., Durrant-Whyte, J., Walters, K.A., Krycer, J.R., et al. (2016). Defining the nutritional and metabolic context of FGF21 using the geometric framework. Cell Metab. *24*, 555–565.

Spergel, D.J., Krüth, U., Hanley, D.F., Sprengel, R., and Seeburg, P.H. (1999). GABA- and glutamate-activated channels in green fluorescent protein-tagged gonadotropin-releasing hormone neurons in transgenic mice. J. Neurosci. *19*, 2037–2050.

Staiger, H., Keuper, M., Berti, L., Hrabe de Angelis, M., and Häring, H.U. (2017). Fibroblast growth factor 21-metabolic role in mice and men. Endocr. Rev. *38*, 468–488.

Talukdar, S., Owen, B.M., Song, P., Hernandez, G., Zhang, Y., Zhou, Y., Scott, W.T., Paratala, B., Turner, T., Smith, A., et al. (2016). FGF21 regulates sweet and alcohol preference. Cell Metab. *23*, 344–349.

Vandanmagsar, B., Warfel, J.D., Wicks, S.E., Ghosh, S., Salbaum, J.M., Burk, D., Dubuisson, O.S., Mendoza, T.M., Zhang, J., Noland, R.C., et al. (2016). Impaired mitochondrial fat oxidation induces FGF21 in muscle. Cell Rep. *15*, 1686–1699.

Véniant, M.M., Komorowski, R., Chen, P., Stanislaus, S., Winters, K., Hager, T., Zhou, L., Wada, R., Hecht, R., and Xu, J. (2012). Long-acting FGF21 has enhanced efficacy in diet-induced obese mice and in obese rhesus monkeys. Endocrinology *153*, 4192–4203.

Véniant, M.M., Sivits, G., Helmering, J., Komorowski, R., Lee, J., Fan, W., Moyer, C., and Lloyd, D.J. (2015). Pharmacologic effects of FGF21 are independent of the "browning" of white adipose tissue. Cell Metab. *21*, 731–738.

Vermaak, W.J., Kalk, W.J., Kuyl, J.M., and Smit, A.M. (1986). Fatty acid induced changes in circulating total and free thyroid hormones: in vivo effects and methodological artefacts. J. Endocrinol. Invest. *9*, 121–126.

Vijayakumar, A., Novosyadlyy, R., Wu, Y., Yakar, S., and LeRoith, D. (2010). Biological effects of growth hormone on carbohydrate and lipid metabolism. Growth Horm. IGF Res. *20*, 1–7.

Violante, I.R., Anastasovska, J., Sanchez-Canon, G.J., Rodrigues, T.B., Righi, V., Nieto-Charques, L., Parkinson, J.R., Bloom, S.R., Bell, J.D., and Cerdán, S. (2009). Cerebral activation by fasting induces lactate accumulation in the hypothalamus. Magn. Reson. Med. *62*, 279–283.

von Holstein-Rathlou, S., BonDurant, L.D., Peltekian, L., Naber, M.C., Yin, T.C., Claflin, K.E., Urizar, A.I., Madsen, A.N., Ratner, C., Holst, B., et al. (2016). FGF21 mediates endocrine control of simple sugar intake and sweet taste preference by the liver. Cell Metab. *23*, 335–343.

Waterson, M.J., and Horvath, T.L. (2015). Neuronal regulation of energy homeostasis: beyond the hypothalamus and feeding. Cell Metab. *22*, 962–970.

Xu, C., Messina, A., Somm, E., Miraoui, H., Kinnunen, T., Acierno, J., Jr., Niederländer, N.J., Bouilly, J., Dwyer, A.A., Sidis, Y., et al. (2017). KLB, encoding beta-klotho, is mutated in patients with congenital hypogonadotropic hypogonadism. EMBO Mol. Med. *9*, 1379–1397.

Yang, C., Jin, C., Li, X., Wang, F., McKeehan, W.L., and Luo, Y. (2012). Differential specificity of endocrine FGF19 and FGF21 to FGFR1 and FGFR4 in complex with KLB. PLoS One *7*, e33870.

Yilmaz, U., Tekin, S., Demir, M., Cigremis, Y., and Sandal, S. (2018). Effects of central FGF21 infusion on the hypothalamus-pituitary-thyroid axis and energy metabolism in rats. J. Physiol. Sci. *68*, 781–788.

Zhang, Y., Xie, Y., Berglund, E.D., Coate, K.C., He, T.T., Katafuchi, T., Xiao, G., Potthoff, M.J., Wei, W., Wan, Y., et al. (2012). The starvation hormone, fibroblast growth factor-21, extends lifespan in mice. ELife *1*, e00065.

Zhang, F., Yu, L., Lin, X., Cheng, P., He, L., Li, X., Lu, X., Tan, Y., Yang, H., Cai, L., et al. (2015). Minireview: roles of fibroblast growth Factors 19 and 21 in metabolic regulation and chronic diseases. Mol. Endocrinol. *29*, 1400–1413.

STAR★METHODS

KEY RESOURCES TABLE

REAGENT or RESOURCE	SOURCE	IDENTIFIER
Antibodies		
Mouse monoclonal Fgf21	Abcam	Cat# ab171941; RRID: AB_2629460
Goat anti-GFP	Sicgen	Cat# AB0020-500; RRID: AB_2333100
chicken anti-Vimentin	Millipore	Cat# AB5733; RRID: AB_11212377
rabbit anti-Glutamine Synthetase	Abcam	Cat# ab73593; RRID: AB_2247588
mouse anti-NeuN	Millipore	Cat# MAB377; RRID: AB_2298772
Alexa Fluor 594-AffiniPure F(ab')2 Fragment Donkey Anti-Rabbit IgG (H+L)	Jackson ImmunoResearch Labs	Cat# 711-586-152; RRID: AB_2340622
Alexa Fluor 647-AffiniPure F(ab')2 Fragment Donkey Anti-Chicken IgY (IgG) (H+L)	Jackson ImmunoResearch Labs	Cat# 703-606-155; RRID: AB_2340380
Alexa Fluor 488-AffiniPure Donkey Anti-Goat IgG (H+L)	Jackson ImmunoResearch Labs	Cat# 705-545-147; RRID: AB_2336933
Cy5-AffiniPure Donkey Anti-Mouse IgG (H+L)	Jackson ImmunoResearch Labs	Cat# 715-175-150; RRID: AB_2340819
Anti-p38 MAPK, phospho (Thr180 / Tyr182) Antibody	Cell Signaling Technology	Cat# 9211; RRID: AB_331641
Anti-p38 MAPK Antibody	Cell Signaling Technology	Cat# 9212; RRID: AB_330713
HSL Antibody	Cell Signaling Technology	Cat# 4107; RRID: AB_2296900
Phospho-HSL (Ser660) Antibody	Cell Signaling Technology	Cat# 4126; RRID: AB_490997
Anti-β-Actin Antibody	Sigma-Aldrich	Cat# A5441; RRID: AB_476744
Sheep Anti-Mouse IgG ECL Antibody, HRP Conjugated,	GE Healthcare	Cat# NA9310-1ml; RRID: AB_772193
Donkey Anti-Rabbit IgG ECL Antibody, HRP Conjugated,	GE Healthcare	Cat# NA9340-1ml; RRID: AB_772191
Sheep Anti-Digoxigenin-AP, Fab fragments	Sigma	Cat# 11093274910; RRID: AB_2734716
Chemicals, Peptides, and Recombinant Proteins		
Palmitate	Sigma	P9767-5G CAS Number 408-35-5
Bovine Serum Albumin Fraction V, fatty acid free	Sigma	10775835001 ROCHE
SB 203580	Sigma	S8307 CAS Number 152121-47-6
TAT-CRE Recombinase	Millipore	SCR508
PAF 32% Aqueous SOL. EM GRADE	Electron Microscopy Sciences	15714-S
DMEM/F-12 (1:1) 1X	ThermoFischer Scientific	31330-038
Fetal Bovine Serum	ThermoFischer Scientific	10270
L-glutamine	ThermoFischer Scientific	25030024
DMEM	ThermoFischer Scientific	A14430-01
D-Glucose	ThermoFischer Scientific	15023-021 CAS Number 50-99-7
Penicillin-Streptomycin	Sigma	P4333
Insulin	Sigma	I1882 CAS Number: 11070-73-8
Putrescine	Sigma	P-7505 CAS Number: 333-93-7
Poly-l-ornithine	Sigma	P3655-100MG CAS Number: 27378-49-0
Neurobasal Medium	ThermoFischer Scientific	12348017
B-27 Supplement	ThermoFischer Scientific	17504001
Glutamax	ThermoFischer Scientific	35050-061
Lipofectamine 3000 Transfection Reagent	ThermoFischer Scientific	L3000015
Opti-MEM Reduced Serum Medium, GlutaMAX Supplement	ThermoFischer Scientific	51985-034
N-acetyl-L-cysteine	Sigma	A7250 CAS Number: 616-91-1
Etomoxir sodium salt hydrate	Sigma	E1905
Sodium oleate	Sigma	O3008-5ML
DL-β-Hydroxybutyric acid sodium salt	Sigma	H6501 CAS Number 150-83-4

(*Continued on next page*)

Continued

REAGENT or RESOURCE	SOURCE	IDENTIFIER
Sodium L-lactate	Sigma	L7022 CAS Number 867-56-1
BODIPY 493/503	ThermoFischer Scientific	D3922
RIPA 10x Lysis Buffer	Millipore	20-188
Protease and Phosphatase Inhibitor	ThermoFischer Scientific	78441B
Tri reagent	Sigma	T9427
RNase-Free DNase Set	Qiagen	79254
SuperScript II Reverse Transcriptase	ThermoFischer Scientific	18064014
GoTaq Long PCR Master Mix	Promega	M4020
Proteinase K	Sigma	SRE0047 CAS Number 39450-01-6
Goat serum	Sigma	G9023
Donkey serum	Sigma	D9663
Skim Milk Powder	Sigma	70166
Carnitine	Sigma	C0158 CAS Number: 541-15-1
Critical Commercial Assays		
Mouse Ultrasensitive Insulin ELISA	Alpco	80-INSMSU-E01
Mouse Glucagon ELISA KitCrystal Chem81518NEFA Non-Esterified Fatty Acids Dosage	IGZ Instruments	434–91795
Quantitative enzymatic determination of glycerol	Sigma	F6428
PrepEase RNA/protein Spin Kit	Affymetrix	PN 78871 1KT
RNeasy Mini Kit	Qiagen	74106
High-Capacity RNA-to-cDNA Kit	ThermoFischer Scientific	4387406
Power Sybr Green PCR master mix	Applied Biosystems	4367659
mouse FGF21 ELisa Kit	Abcam	212160
DCFDA - Cellular Reactive Oxygen Species Detection Assay Kit	Abcam	ab113851
BCA Protein Assay kit	ThermoFischer Scientific	23225
Micro BCA Protein Assay kit	ThermoFischer Scientific	23235
Reversible protein stain kit-for nitrocellulose membranes	ThermoFischer Scientific	24580
WesternBright Sirius- femtogram HRP Substrate	Witec	K-12043-D20
WesternBright ECL- femtogram HRP Substrate	Witec	K-12045-D50
Experimental Models: Cell Lines		
3T3-L1 cell line	Laboratory of Lluis Fajas	Cat# CCL-92.1; RRID: CVCL_0123
Experimental Models: Organisms/Strains		
Mouse: C57BL/6 *Fgf21 KO*	Laboratory of Nelly Pitteloud; Hotta et al. (2009)	N/A
Mouse: C57BL/6 *Klb KO*	Laboratory of Nelly Pitteloud; Ito et al. (2005)	N/A
Mouse: C57BL/6 *Gnrh-Gfp*	Laboratory of Vincent Prévot; Spergel et al. (1999)	N/A
Mouse: C57BL/6 *Npy-Gfp* mice	Laboratory of Corinne Leloup; Pinto et al. (2004)	Cat# JAX:008321; RRID: IMSR_JAX:008321
Mouse: C57BL/6J dtomato$^{fl/fl}$ mice (B6.Cg-*Gt*(ROSA)*26Sor*$^{tm9(CAG\text{-}tdTomato)Hze}$/J)	The Jackson Laboratory; Madisen et al. (2010)	Cat# JAX:007909; RRID: IMSR_JAX:007909
Mouse: C57BL/6J Fgf21$^{fl/fl}$ mice (B6.129S6(SJL)-*Fgf21*$^{tm1.2Djm}$/J)	The Jackson Laboratory; Potthoff et al. (2009)	Cat# JAX:022361; RRID: IMSR_JAX:022361
Mouse: C57BL/6J Mus musculus	The Jackson Laboratory	Cat# JAX:000664; RRID: IMSR_JAX:000664
Oligonucleotides		
siRNA FGF21 silencer select	Ambion	4390771
siRNA scramble FGF21 silencer select	Ambion	4390843
Primers for RT-qPCR are listed in Table S1	This paper	N/A

(*Continued on next page*)

Continued		
REAGENT or RESOURCE	SOURCE	IDENTIFIER
Recombinant DNA		
Plasmid: 3xFlag-Fgf21	This paper	N/A
Plasmid: GFP-Fgf21	This paper	N/A
Empty vectors pci-3xFlag	Dr. Yoan Arribat	N/A
Empty vectors pDest53-GFP plasmid	Dr. Yoan Arribat	N/A
Software and Algorithms		
GraphPad Prism 7.03	GraphPad Prism	https://www.graphpad.com/scientific-software/prism/
ImageJ	Schneider et al., 2012	https://imagej.nih.gov/ij/
Zen software	Zeiss	https://www.zeiss.fr/microscopie/produits/microscope-software/zen-lite/zen-2-lite-download.html
Seahorse Wave Desktop Software	Agilent	https://www.agilent.com/en/products/cell-analysis/cell-analysis-software/data-analysis/wave-desktop-2-6
Other		
Mini-Protean TGX Precast Gels 8-16%-15well-15ul	Biorad	456-8106

LEAD CONTACT AND MATERIALS AVAILABILITY

Further information and requests for resources and reagents should be directed to Luc Pellerin (luc.pellerin@unil.ch).

EXPERIMENTAL MODEL AND SUBJECT DETAILS

Animals

Male mice, 3–4 months old, were maintained in a temperature-controlled animal facility with a 12-hour light/dark cycle and had access to food and water *ad libitum*. All procedures were approved by the Swiss ''Service de la Consommation et des Affaires Vétérinaires du Canton de Vaud'' (SCAV, authorization n°2634.1 and n°3229.a). Male C57Bl/6RJ mice were purchased from Janvier Labs (Le Genest-Saint-Isle, France). The generation and genotyping of C57BL/6 *Fgf21 KO* mice and C57BL/6 *Klb KO* mice were previously described by Hotta et al. (2009) and Ito et al. (2005). The generation of C57BL/6 *Gnrh-Gfp* mice and *Npy-Gfp* mice were previously described by Spergel et al. (1999) and Pinto et al. (2004). The C57BL/6J dtomato$^{fl/fl}$ mice (B6.Cg-*Gt*(ROSA) *26Sor*$^{tm9(CAG-tdTomato)Hze}$/J), C57BL/6J *Fgf21*$^{fl/fl}$ mice (B6.129S6(SJL)-*Fgf21*^{tm1}.^{2Djm}/J) and C57BL/6J *Fgf21*$^{+/+}$ mice (controls recommended by Jackson Labs) were bought from Jackson labs. The generation of C57BL/6J *Fgf21*$^{fl/fl}$ mice were previously described by Potthoff et al. (2009) and Markan et al. (2014).

Fasting Test

For fasting/refeeding experiments, C57Bl/6RJ mice, 3–4 months old, were fasted for 24h or fasted for 18h and refed 6h before collecting tissues.

Treatment Protocols and Stereotaxic Surgery

Palmitate (Sigma, Buchs, Switzerland) coupled to fatty acid free BSA (Roche-Sigma, Buchs, Switzerland) was used at 100μM final concentration, pH 7.4 (Lopez-Mejia et al., 2017). C57Bl/6RJ mice fed *ad libitum* (3 months old) were given an i.v. injection of 150μl of saline Palmitate or an equal volume of saline BSA (control) in the tail. Stereotaxic injections of saline SB203580 (10μM) or saline DMSO into the third ventricle using a cannula guide were performed as described below. Adult mice were anesthetized with 0.5–2.0 % isoflurane in 95 % O_2/5 % CO_2 mixture, placed in a stereotaxic frame, and implanted with a cannula guide (0.60/0.40 x 10 mm, Unimed S.A.) in the third ventricle (coordinates from bregma: AP -2.3 mm, 0mm from midline, DV -4.7mm). The cannula guide was fixed to the skull with dental cement. After surgery, anesthesia was discontinued, and mice were returned to their cage and provided with food and water *ad libitum*. One week after surgery, the animals were briefly anesthetized to introduce an inner cannula (0.25/0.16 x 11 mm) to inject into the third ventricule (final ventral coordinate -5.7) 2μl of saline SB203580 (10μM, Sigma, Buchs, Switzerland) coupled to fatty acid free BSA (Roche-Sigma, Buchs, Switzerland) was used at 100μM final concentration) or an equal volume of saline DMSO at a speed of 0.4 μl/min. One hour after this intraventricular injection, mice received i.v. tail injection of saline palmitate or BSA. The intraventricular injection of only 1μl of the corresponding treatments was repeated 5, 11 and

17 h after the i.v. treatment. During all this time, mice were provided with food and water *ad libitum*. 20 h after the i.v. treatment, mice were sacrificed by cervical dislocation and their tissues were collected for further analysis.

TAT-CRE recombinase protein (Millipore, Zug, Switzerland) was used at 2mg/ml and injected into the third ventricle (AP -2.3 mm, 0mm from midline, DV -5.7mm) of dtomato$^{fl/fl}$, *Fgf21*$^{fl/fl}$ and *Fgf21*$^{+/+}$ mice (3-4 months old) using a cannula as described above. After surgery, mice were returned to their cage and provided with food and water *ad libitum*. Two weeks after surgery, *Fgf21*$^{fl/fl}$ and *Fgf21*$^{+/+}$ mice were fasted during 24h and sacrificed by cervical dislocation. Their tissues were collected for further analysis. dtomato$^{fl/fl}$ mice were perfused with PAF 4% two days after TAT-CRE injection, and brains were removed and processed for confocal analyses.

Physiological Measurements

Experimental procedure timeline before and after TAT-CRE injection in 3V of *Fgf21*$^{+/+}$ and *Fgf21*$^{fl/fl}$ mice is detailed in Figure S4G.

Body composition measurement was performed using EchoMRI (LLC., Houston, Texas) in C57BL/6J Fgf21$^{fl/fl}$ mice and C57BL/6J Fgf21$^{+/+}$ mice aged 10-13 weeks old. Analysis for total energy expenditure, oxygen consumption and voluntary locomotion was performed using indirect calorimetry measurements (Promethion, Sable Systems International, Berlin, Germany). Mice were individually housed and acclimatized to the cages for 24h before experimental measurements. Food intake was measured manually. Whole body fatty acid oxidation (FAO) was calculated using the formula FAO=EE(1-RER/0,3) (Bruss et al., 2010). Ketone bodies (β-hydroxybutyrate, Free Style Precision; Abbott, Baar, Switzerland) and glucose concentrations (Benecheck plus Multi-monitoring system; Benecheck, Hasselt, Belgium) were measured from blood taken from the tail vein using the indicated kit. For PTT, GTT and GSIS, mice were starved for 16 hours and then injected i.p. with pyruvate (1.5g/kg) or glucose (2g/kg). Insulin (Alpco, Bühlmann Laboratories AG, Schönenbuch, Switzerland), glucagon (Crytal chem, Zaandam, Netherlands) NEFAs (IGZ Instruments, Zürich, Switzerland) and Glycerol (Sigma, Buchs, Switzerland) were measured from serum. The quantitative insulin sensitivity check index (QUICKI) was calculated using the formula QUICKI=1/log ((16h fasting insulin μU/mL) + log (16h fasting glucose mg/dL)) (Berglund et al., 2008).

Cell Culture

Primary Cell Culture Experiments

Unless otherwise stated, all chemicals were purchased from Invitrogen (Lucerne, Switzerland).

Primary cell cultures were prepared from OF1: SWISS mice (Janvier Laboratories, France) according to the SCAV authorization (n°1251.5).

Tanycytes were prepared from ARC/ME dissected from 8-10-day-old female and male pups according to the punches protocol described below (see Method Details - Brain, Liver and scWAT Sample Processing). After a growing period of 18-21 days in 75 cm^2 culture flasks containing DMEM/F12 high-glucose medium supplemented with 10% fetal calf serum and 2mM L-glutamine, tanycytes were isolated from contaminant cells by shaking and plated in wells of different diameters depending of the type of experiment. After reaching 90% confluence, the medium was replaced with a serum-free medium for glia composed of DMEM devoid of phenol red, supplemented with 1mM Glucose and 2mM L-glutamine. The cells were used 48 h later for experiments.

Astrocytes were isolated from the hypothalamus of 2-days old pups (female and male) and cultured as previously described by Prevot et al. (2003). Astrocytes were grown during 18-21 days in 75cm^2 flask containing DMEM/F12 medium supplemented with 10% fetal calf serum, 1% L-Glutamine and 1% penicillin/streptomycin (P/S). Cells were then seeded in 35mm ø dishes. After reaching 90% confluence, the cells were incubated two days in astrocyte-defined medium composed of DMEM (5mM Glucose, devoid of phenol red) supplemented with 1% L-glutamine, 5μg/ml insulin (Sigma, Buchs, Switzerland) and 100μM Putrescine (Sigma, Buchs, Switzerland).

Primary cultures of hypothalamic neurons were prepared from embryonic day 17 (E17) mice (female and male). Neurons were purified as described by Allaman et al. (2010). Cells were plated at an average density of 35×10^4 cells/well (35 mm ø) coated with poly-ornithine (25mg/l; Sigma, Buchs, Switzerland) in Neurobasal medium (25mM of Glucose) supplemented with 2% B-27, 1% Glutamax and 1% P/S. At day 3, 1μM of Cytosine arabinoside (*AraC*, *Sigma*, Buchs, Switzerland) was added in the culture medium. At day 9 the medium was changed 3:4 with DMEM (devoid of Glucose, phenol red) supplemented with 1% Glutamax. Neurons were used at day 10 for the experiment.

The cultures were maintained in a water-saturated atmosphere at 37°C with 5% O_2:95% CO_2.

cDNA/siRNA Transfection and Cell Treatments

3T3-L1 adipocytes were cultured as described by Lagarrigue et al. (2016). 3T3-L1 mature adipocytes transfected with different concentrations of Small interfering RNA (siRNA) against Fgf21 were used to characterize its specificity, as described below. siFgf21 (20-200nM for 3T3-L1 cells and 75 nM for tanycytes; Ambion, ThermoFisher Scientific, Basel, Switzerland) and cDNA of 3xFlag-Fgf21 or GFP-Fgf21 (1.5μg) were transfected using Lipofectamine TM 3000 reagent (Invitrogen, ThermoFisher Scientific, Basel, Switzerland) prepared in Opti-MEM/GlutaMax (Invitrogen, Basel, Switzerland) and DMEM/F12 medium without antibiotic according to the manufacturer's instructions. After 12h of incubation, the transfection medium was replaced with serum-free medium for glia. Tanycytes were harvested 24h or 48h after the beginning of transfection for RNA analysis or protein analysis respectively. siRNA recommended by the manufacturer (20-200nM for 3T3-L1 cells and 75 nM for tanycytes; Ambion, ThermoFisher Scientific, Basel, Switzerland) and empty vectors (pci-3xFlag or pDest53-GFP plasmid) have been used as negative controls.

Tanycytes were treated with palmitate coupled to fatty acid free BSA (100μM, pH7.4) during the indicated times with or without N-acetyl-L-cysteine (NAC, 1mM, Sigma, Buchs, Switzerland) or etomoxir (200μM, Sigma, Buchs, Switzerland). Cells were pre-treated one hour before palmitate stimulation with p38-MAPK Inhibitor SB203580 (10μM, Sigma, Buchs, Switzerland). Control samples were incubated with BSA/Ethanol and/or DMSO depending of the treatment. Tanycytes were also treated with oleate coupled to fatty acid free BSA (250μM, pH7.4, Sigma, Buchs, Switzerland), BHB (20mM, pH7.4, Sigma, Buchs, Switzerland) and Lactate (20mM, pH7.4, AxonLab, Baden, Switzerland). After indicated times of treatment, cells were collected for RT-qPCR or western blot analysis.

To label lipid droplets, cells were incubated with BODIPY 493/503 (1/1000, Life Technology, ThermoFisher Scientific, Basel, Switzerland) during the last 30min of treatment and then fixed with PAF 4% during 30min.

METHOD DETAILS

Brain, Liver and scWAT Sample Processing

All procedures for brain, liver and scWAT dissections were performed under RNAse-free conditions. Mice were dislocated, liver and brain were quickly removed. Hypothalami were isolated or punches were prepared. Brains were placed in a cold dissection matrix to isolate 1 mm slices and brain slices were placed under a binocular microscope (Leica MZ6) to quickly dissect different hypothalamic areas and the barrel cortex. Punches were immediately homogenized on ice in 350μl of lysis buffer and stored at -80°C. Liver and hypothalamic samples were directly frozen using liquid nitrogen and stored at -80°C. Brain fixation was performed as described by Geller et al. (2017). Brains were conserved at -80°C until being cut (30μm thick) with a cryostat (CM 3050S; Leica Biosystems, Dusseldorf, Germany).

RNA and Protein Purification

Liver or hypothalamic samples and punches were lysed and homogenized in 350μl of RP1 lysis Buffer (PrepEase RNA/Protein Spin Kit, Affymetrix, Staufen, Germany). Total RNA was isolated on spin columns and then digested with DNase supplied in the Kit. RNA was eluted with water, 60μl for liver/hypothalami and 40μl for punches. Proteins were precipitated according to the manufacturer's instructions and recovered in 100μl (liver/hypothalamic) or 20μl (punches) of RIPA lysis buffer (Millipore, Zug, Switzerland) completed with protease/phosphatase inhibitors (Thermo scientific Reinach, Switzerland). scWAT samples were lysed and homogenized in 500 μl of Tri-Reagent (Sigma, Buchs, Switzerland). Total RNA was isolated according to the manufacturer's protocol and dissolved in 30μl of water. Total RNA from primary cultures was purified using the RNeasy Mini Kit, (Qiagen, Basel, Switzerland) according to the manufacturer's instructions. RNA was digested with DNase (RNase-Free DNase Set, Qiagen, Basel, Switzerland) and eluted with 20μl of water. Proteins were extracted with 40μl of RIPA lysis buffer.

RNA concentrations were determined with a Nanodrop (ND-1000 Spectrophotometer, Witec, Luzern, Switzerland). Protein concentrations were determined using Micro BCA TM Protein assay kit (Invitrogen, ThermoFisher Scientific, Basel, Switzerland), according to the manufacturer's instructions

RT-PCR and Plasmid Cloning

mRNA and protein nomenclatures are in accordance to Cell Press editorial Policies (http://www.cell.com/trends/editorial-policies).

Mouse mRNAs (600ng, 1,000ng for liver and hypothalamus respectively and 2,000ng for tanycyte cultures) were reverse transcribed using SuperScript TM II Reverse Transcriptase Kit (Invitrogen, Thermo Fisher Scientific, Waltham, USA). cDNAs of *Fgf21* were amplified by PCR with Gotaq long PCR master mix (Promega, Dübendorf, Switzerland) using 1μl and 6μl of cDNA (from liver and hypothalamus/tanycytes respectively). The construct was generated using the Gateway system with the mFgf21 sequence isolated *in vivo* and cloned under a CMV promoter, which exhibits a tropism for glia. Primers flanked with ATTB1/ATTB2 sequences were used for subsequent cloning of *mFgf21* in the pci-3xFlag or pDest53-GFP backbone vectors: Forward: ggggacaagtttgtacaaaaaagcaggcttcATGGAATGGATGAGATCTAGA and Reverse: ggggaccactttgtacaagaaagctgggttGGACGCATAGCTGGGGCTTCG. Primer sequences for detecting *Fgf21* mRNA full transcript were: Forward: ATGGAATGGATGAGATCTAGA and Reverse: GGACGCATAGCTGGGGCTTCG. *Gapdh* mRNA was used as an endogenous control Forward: TGTTGAAGTCGCAGGAGACAAC and Reverse: CACCATCTTCCAGGAGCGAG. Sequence analysis was performed by Microsynth AG (Balgach; Switzerland).

RT-qPCR

RNA reverse transcription and Real-Time PCR were performed as described by Carneiro et al. (2016). Briefly, RNA was reverse transcribed using the RT High Capacity RNA-to-cDNA Kit (Applied Biosystems, Rotkreuz, Switzerland). Real-Time PCR analysis was performed on 1μl to 3μl of cDNA and using Power SYBR Green Taq polymerase master mix (Applied Biosystems, Rotkreuz, Switzerland). Primer sequences used for mRNA quantification were directed against *Fgf21, Klb, Fgfr1c, Gnrh, Kiss, Npy, Agrp, Rbfos3, Glul* mRNA as well as polymerase 2a *Polr2a* mRNA which was used as an endogenous control (See Table S1).

Fgf21 ELISA Measurement

Fgf21 secretion was analyzed from cell culture supernatant using mouse Fgf21 ELISA Kit (Abcam, Cambridge, UK) according to the manufacturer's instructions. Intensity was read at 450nm using a microplate reader (Sinergy MX, Biotech). Proteins were collected and quantified as described in the protein purification section to normalize the values to the total protein content.

ROS-Oxidized DCF Measurement

ROS production was detected by fluorescence emitted by ROS-oxidized DCF using DCFDA - Cellular Reactive Oxygen Species Detection Assay Kit (1/2000, Abcam, Cambridge, UK) following the manufacturer's instructions. After 30min of DCFDA incubation, cells were washed and incubated with NAC and/or palmitate before performing Time-lapse analysis using a confocal microscope (inverted Zeiss LSM 710 confocal microscope) or quantitative analysis using a Fluorescence microplate reader (Sinergy MX, Biotech) at Excitation 495nm and Emission 529nm wavelengths. Proteins were collected and quantified as described in the protein purification section to normalize fluorescence emission to the total protein content.

In Situ Hybridization

In situ hybridization was performed using the established protocol of Liang et al. (2000). Sense and antisense probes were amplified by PCR, and directly transcribed thanks to T7 promoter sequence (lower case) inserted in forward primers: T7-Fgf21 Forward: gaaattaatacgactcactatagggATGGAATGGATGAGATCTAGA, T7-Fgf21 Reverse: gaaattaatacgactcactatagggGCAGGAAGCGCAC AGGTCCCC, Fgf21 Forward: ATGGAATGGATGAGATCTAGA and Fgf21 Reverse: GCAGGAAGCGCACAGGTCCCC. The Fgf21 probes encompassed the first 499 base pair region of the Fgf21 mRNA. Coronal brain sections were digested with Proteinase K (20μg/ml, Sigma, Buchs, Switzerland) in PBST during 30s. Prehybridization was performed at 70°C during 2h. Hybridization was performed with 2ng/μl of probes at 70°C overnight. Slices were incubated in blocking buffer during 30min at Room Temperature (RT) and then in anti-DIG antibodies (1/2000, Roche, Basel/Kaiseraugs, Switzerland) diluted in PBST 2% goat serum (Sigma, Buchs, Switzerland) at 4°C overnight and at RT during 6h. Image acquisitions were performed using a binocular microscope (Leica MZ6).

Immunofluorescence

Immunofluorescence labelings were performed essentially as previously described by Geller et al. (2017). For Fgf21 immunoreactivity detection, coronal brain sections were incubated in Citrate Buffer pH 6 during 15min at RT and heated at 60°C and 90°C during 2min for each temperature. Coronal brain sections or primary cultures were incubated with primary antibody rabbit monoclonal anti-Fgf21 (1/100, Abcam, Cambridge, UK) during three nights at 4°C and/or goat anti-GFP (1/1000, Sicgen, Carcavelos - PORTUGAL), chicken anti-Vimentin (1/2000, Millipore, Zug, Switzerland), rabbit anti-Glutamine Synthetase (1/1000, Sigma, Buchs, Switzerland) and mouse anti-NeuN (1/500, Millipore, Zug, Switzerland) overnight at 4°C. Secondary antibody anti-rabbit AF594, anti-chicken AF647 (F(ab')2 fragment from donkey, Jackson Immunoresearch, Suffolk, UK) and donkey anti-goat AF488, donkey anti-mouse Cy5 (IgG (H+L), Jackson Immunoresearch, Suffolk, UK) were incubated 2h at RT. Fluorescence images were captured using an inverted Zeiss LSM 710 confocal microscope using tile scan mode.

Hematoxylin and Eosin Staining

Liver and scWAT hematoxylin and eosin stainings were performed essentially as described by Carneiro et al. (2017). Liver and scWAT were paraffin-embedded and 3mm tissue sections were prepared. Each section was stained with hematoxylin and eosin and examined with a Nikon Eclipse 80i microscope (Nikon AG, Egg, Switzerland) using brightfield optics at x20 and x40 magnification. The number of lipid droplets was quantified using Image J 1.52a software (NIH) on x20 magnification pictures (two pictures for each animal).

Western Blot Analysis

Western blots were performed essentially as described by Carneiro et al. (2016). Proteins (in a volume of 20μl) were separated with 10% or 15% of homemade SDS-PAGE or 8-16% precast gels (Bio-Rad). After transfer on nitrocellulose membranes, detection of protein transfer efficiency was performed using MemCode Reversible Protein Stain Kit (ThermoFisher Scientific, Basel, Switzerland) according to the manufacturer's instructions. Membranes were incubated in blocking buffer composed of TBST 5% nonfat milk (Sigma, Buchs, Switzerland) during 30min at RT. Then, membranes were incubated with primary antibody Rabbit anti-Fgf21 (1/500, Abcam, Cambridge, UK) two nights at 4°C or Rabbit anti p38-MAPK, Rabbit anti phospho-P38-MAPK, Rabbit anti-Hsl, Rabbit anti phospho-Hsl (Cell Signaling, Beverly, MA, USA), goat anti-GS (1/1000, Millipore, Zug, Switzerland), mouse anti-NeuN (1/500, Millipore, Zug, Switzerland) or mouse anti-actin (1/5000, Sigma, Buchs, Switzerland) were incubated overnight at 4°C. Proteins were detected using an incubation of 2h at RT with goat anti-rabbit or goat anti-mouse peroxidase-conjugated secondary antibody (1/5,000; GE Healthcare, Piscataway, NJ, USA) or rabbit anti-goat (1/5,000; Jackson Immunoresearch, Suffolk, UK). Bands were revealed with a chemiluminescence kit ECL or Sirius (BioRad, Reinach, Switzerland) and processed with a ChemiDoc XRS system (BioRad, Reinach, Switzerland) for densitometry analysis. Western blots were normalized to total protein levels using Memcode. Figure panels composed of independent membranes are indicated with vertical lines.

Seahorse Analysis

FAO analysis was performed as described by Lopez-Mejia et al. (2017). For seahorse analysis, cells were seeded 4 days before the experiment in XF24-wells cell culture microplates coated with poly-L-ornithine (15mg/ml, Sigma, Buchs, Switzerland) at a density of 6×10^4 cells per well in 200μL DMEM/F12 media. After 48h, the medium was replaced with a serum-free medium for tanycytes. Cells were incubated two days more at 37°C in 5% CO_2 before the assay. Oxygen Consumption Rate (OCR) was measured in adherent tanycytes with an XF-24 extracellular flux analyzer (Seahorse Bioscience). Just before the experiment, cells were washed and the medium was replaced with Krebs-Henseleit Buffer (KHB) containing 2.5mM Glucose and 1.5mM of carnitine. Cells were then pre-incubated for 1hr at 37°C without CO_2 to allow cells to pre-equilibrate with the assay medium before starting the fatty acid oxidation procedure. After measuring baseline OCR as an indication of basal respiration, OCR was measured after an acute injection of 100μM of palmitate coupled to BSA and 200μM of etomoxir. OCR was expressed as pmol of O_2 per minute and was normalized by protein content which was measured with a Pierce BCA Protein Assay protocol (Thermo Fisher Scientific). The experiments were realized on 28 wells from two independent cultures.

QUANTIFICATION AND STATISTICAL ANALYSIS

Data were analyzed on GraphPad Prism 7.03. Animals that lost 15% body weight (5% fat mass) the week after surgery were excluded from the study. For *in vivo* studies, the "n" indicated in figures legends corresponds to the number of animals per group. For *in vitro* studies, the experiments were performed on three independent cultures (N = 3) and at least on three wells per culture (n = 3), except stated otherwise in the figures legends. Statistical details are indicated in the figure legends. After verification of the normal distribution of the data, one-way ANOVA followed by Tukey's HSD (Honest Significant Different) test for multiple comparisons or by one way ANOVA followed Dunnett's for multiple comparison with the single control were performed. Differences between two groups were analyzed using unpaired Student's t-tests or Mann-Whitney tests. P value $\leq$ 0.5 have been considered as significant. Data are expressed as mean ± SEM.